Preparation and characterization of carbonated high-calcium fly ash as supplementary cementitious material

Ge, Zhi; Xue, Xingjie; Fang, Haibo; Shao, Yingxuan; Sun, Ke; Zhang, Hongzhi; Šavija, Branko

DOI
10.1016/j.conbuildmat.2025.140285

Publication date
2025

Document Version
Final published version

Published in
Construction and Building Materials

Construction and Building Materials 466 (2025) 140285

Contents lists available at ScienceDirect

Construction and Building Materials

journal homepage: www.elsevier.com/locate/conbuildmat

Preparation and characterization of carbonated high-calcium fly ash as supplementary cementitious material

Zhi Ge [a,c], Xingjie Xue [a,c], Haibo Fang [b,c], Yingxuan Shao [a,c], Ke Sun [a,c], Hongzhi Zhang [a,c,*], Branko Šavija [b,c]

[a] School of Qilu Transportation, Shandong University, Jinan 250002, China
[b] The Second Construction Limited Company of China Construction Eighth Engineering Division, Jinan 250014, China
[c] Microlab, Faculty of Civil Engineering and Geosciences, Delft University of Technology, Delft 2628 CN, the Netherlands

ARTICLE INFO

Keywords:
CO_2 carbonation
High-calcium fly ash
Krstulovic-Dabic model
Hydration product

ABSTRACT

This paper aims to improve the activity of high-calcium fly ash (FA) by using a wet carbonation treatment process. The results indicated that carbonation products, i.e. calcite, were attached to the surface of FA, which accelerated cement hydration primarily at the early stage. Significant improvement of early age strength and a decrease in setting time were therefore found in blended cement. Additionally, carbonation significantly reduced the amount of free calcium oxide (f-CaO) in FA, increasing its volume stability. Krstulovic-Dabic model was used to simulate the hydration process of blended paste, and the distribution of pore sizes and hydration products were also measured. Together with the filler effect of nano-sized calcite, the formation of carboaluminate phases refined the pore structure of blended paste. Furthermore, the amounts and mechanical properties of outer hydration products in blended paste increased.

1. Introduction

Cement is indispensable for infrastructure construction, but its production puts a high energy demand and produces significant emissions of CO_2 [1]. Cement production emits 500–700 kg of CO_2 per ton [2]. The global cement production was expected to be 4.1×10^{12} kg in 2020 [3]. Consequently, it is vital to diminish CO_2 emissions from the cement business to avert the exacerbation of the worldwide greenhouse effect [4]. Substituting cement with supplemental cementitious materials (SCMs) like fly ash (FA) is regarded as one of the primary technical approaches to mitigate carbon emissions. According to the calcium content in FA, it can be classified as class C and class F [5]. The CaO content in class C FA exceeds 10 %. In general, class C FA has higher activity than class F FA. In practice, no more than 20 % replacement levels are used even though FA provides economic and environmental benefits [6]. One of the reasons is the low activity of FA, which significantly reduces the early strength and delays the setting. Furthermore, there is a significant amount of free calcium oxide (f-CaO) in class C FA, resulting in local expansion and volume stability issues. Therefore, improving the volume stability and reactivity of class C fly ash to increase the replacement ratio in cementitious materials is essential for reducing carbon emissions in the concrete and cement industry. [7–10].

Efforts have been made to reduce the content of f-CaO in FA, such as disintegration [11], grinding [12,13], and using additives [14]. However, these methods have some disadvantages, such as the low conversion efficiency of f-CaO and the limited activity of FA pre-treatment. An alternative approach is carbonation treatment in which f-CaO in FA will react with CO_2 to form $CaCO_3$ [15,16]. Typically, the carbonation approach involves two categories [17–19]: direct and indirect. There are two types of direct carbonization: dry and wet. In dry carbonation process, the CO_2 gas phase interacts directly with a solid phase to produce carbonate [20]. According to [21–23], dry carbonation was conducted using a gas-solid approach that lasted more than a few hours. The efficiency is possibly insufficient for industrial applications [21]. Deng et al. [24] treated FA through a gas-solid accelerated carbonation, and the reaction time was 12 h with a carbonization efficiency of around 27 %. Tamilselvi et al. [25] reported that increasing CO_2 pressure could improve the carbon gain of FA, but the reaction is slow. The maximum sequestration capacity is 26.3 kgCO_2/t solid waste at 10 bar for 1 hour. Liu [26], Cwik and Rausis [27] introduced steam into the reaction, significantly improving the carbon sequestration capabilities of FA, reaching 101 kg CO_2/t FA. Dry carbonation can improve the reaction

* Correspondence to: .Jinan 250002, China.
E-mail address: hzzhang@sdu.edu.cn (H. Zhang).

https://doi.org/10.1016/j.conbuildmat.2025.140285
Received 4 December 2024; Received in revised form 18 January 2025; Accepted 2 February 2025
Available online 7 February 2025

Table 1
Chemical composition of raw materials (wt%).

Component	SiO_2	Al_2O_3	Fe_2O_3	CaO	MgO	SO_3	Others	LOI
OPC	21.82	4.68	3.56	63.43	3.29	2.30	0.92	1.48
FA	43.00	24.60	4.61	20.91	2.42	0.84	3.62	4.76

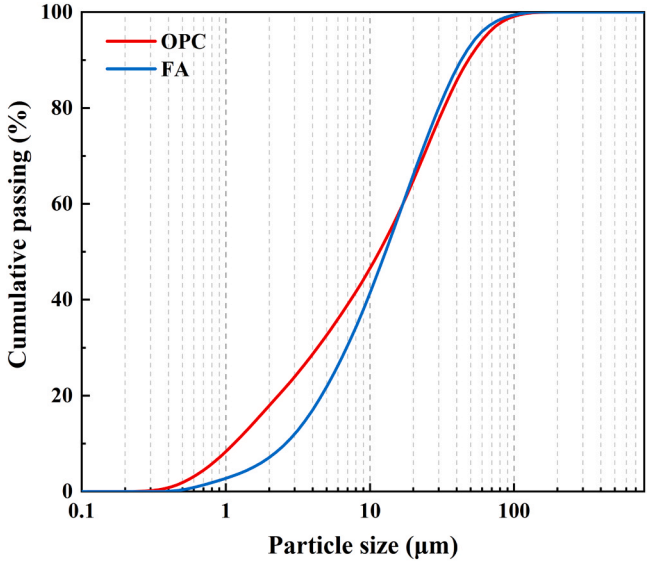

Fig. 1. Distribution of particle sizes in raw materials.

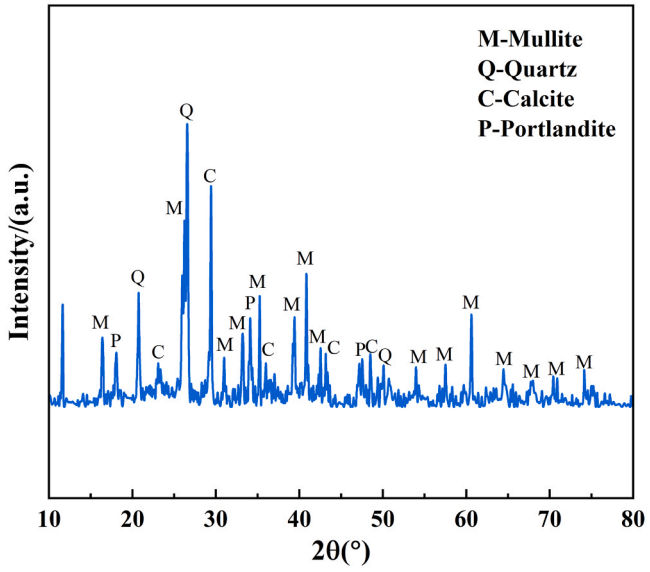

Fig. 2. XRD patterns of FA.

rate through high temperature or pressure, which leads to a remark increase in production energy consumption.

To improve the carbon sequestration capabilities of FA, many researchers used wet carbonation [25,28]. In this approach, alkaline solid waste is mixed with water so that the active substances in solid waste are dissolved into alkali metal ions. Then CO_2 is electrolyzed into CO_3^{2-}/HCO_3^- ions and combined with metal ions to form carbonate. The FA carbonization process commonly covers a broad range of reaction conditions. The reported reaction temperature ranges from 25℃ to 275℃ and the pressure is in between 1 and 80 bar [26,29–31]. The reaction temperature only enhances the early carbonation efficiency without significantly affecting the overall carbon sequestration. The carbon sequestration rate is between 10.71 and 27.05 $kgCO_2$/t solid waste [32]. Improved pressures of CO_2 can significantly influence the carbon sequestration of FA, as higher pressure favors the leaching rate of calcium ions. The CO_2 sequestration capacity rises from 35.48 kg/t (5 bar) to 67.92 kg/t (25 bar), with an increase of 91.4 % [33]. Recently, some researchers modified FA using mechanical methods to enhance its reactivity during carbonation [34]. However, pre-treatment also results in higher energy and economic costs.

To this end, this study developed a wet carbonation process under normal temperature and pressure to prepare carbonated high-calcium fly ash (CFA) within 10 min. The CO_2 uptake capacity of FA was measured, and features of the CFA were characterized. Cement pastes prepared with different replacement rates of CFA (20, 30 %, 40 %, and 50 %) were evaluated regarding volume stability, workability, setting time and mechanical properties. Mechanisms behind were investigated to guide the implementation of CFA as a new SCM.

2. Materials and methods

2.1. Raw materials

In this study, P.I. 42.5 standard ordinary Portland cement (OPC) and ASTM Class C fly ash [35] were utilized as raw materials. The density of OPC was 3.11 g/cm^3 and its specific surface area was 358 m^2/kg. The Blaine fineness of Class C fly ash (FA) was 343.2 m^2/kg. Table 1 presents the chemical composition of the raw materials, and the particle size distribution is shown in Fig. 1. The content of CaO and SiO_2 in FA is 20.91 % and 43 %, respectively, whereas the f-CaO content in FA is 5.51 %. X-ray diffraction (XRD) of the raw materials is shown in Fig. 2. Portlandite and calcite are found in FA. Calcite formation in FA occurs because f-CaO reacts with carbon dioxide during storage [36].

2.2. Preparation and characterization of carbonated FA

As shown in Fig. 3, FA was carbonated using direct wet carbonation at 20°C. Solids were first mixed with water using a magnetic stirrer switch in direct wet carbonation. A liquid-to-solid ratio of 7.5 was selected to guarantee the maximum carbonization efficiency. The pH was monitored during mixing and carbonation. Once the pH was stabilized, CO_2 was infused into the mixture at a speed of 0.4 L/min. The injection of CO_2 was stopped when the pH value reached 7.0, which lasted about 6 min. The mixtures were then passed through a 0.1 μm filter and subjected to vacuum drying at 40℃ for 24 hours.

A laser particle size analyzer was utilized to assess the distribution of particle sizes in CFA, covering a range from 0.02 to 2000 mm. The crystalline composition and microstructure were investigated using measurements like X-ray powder diffraction (XRD), thermogravimetric analysis (TGA), Fourier transform infrared spectroscopy (FTIR), and scanning electron microscopy (SEM). The specific setup is described in section 2.4.8. The f-CaO concentration of class C FA was determined by phenyl formic acid titration following Chinese standard GB/T 176–2008.

2.3. Preparation and characterization of blended OPC-FA/CFA pastes

2.3.1. Mix proportion and sample preparation

Samples of cement paste measuring 40 mm × 40 mm × 40 mm were made in the lab at 20°C and allowed to cure for 24 hours in molds. The

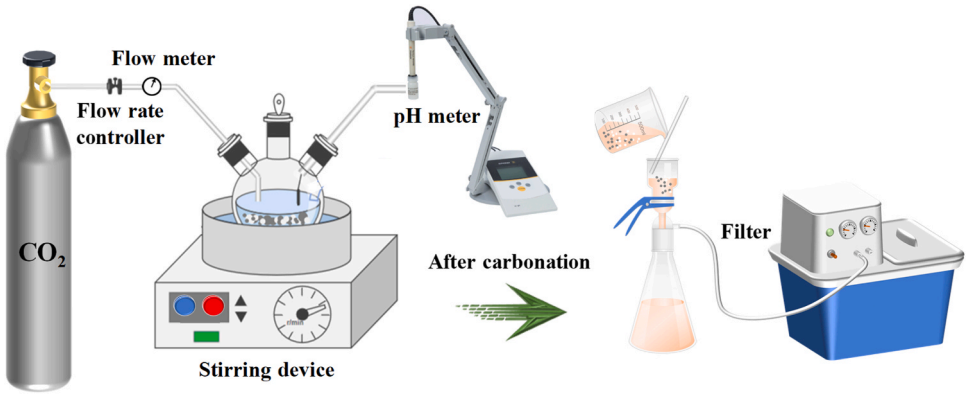

Fig. 3. Schematics of the experimental setup used for aqueous carbonation.

Table 2
Mix proportions of blended cement pastes.

Samples	OPC content (wt%)	FA type	FA content (wt%)	w/b
OPC	100	-	0	0.40
FA20	80	FA	20	0.40
FA30	70	FA	30	0.40
FA40	60	FA	40	0.40
FA50	50	FA	50	0.40
CFA20	80	CFA	20	0.40
CFA30	70	CFA	30	0.40
CFA40	60	CFA	40	0.40
CFA50	50	CFA	50	0.40

paste samples were demolded and cured in a wet atmosphere (temperature = 20 °C; relative humidity > 95 %) until test age. The blended mixes consisted of OPC and 20 %-50 % FA/CFA by weight. Table 2 shows the mix proportion, pure OPC paste was used as a reference.

2.3.2. Setting time

According to ASTM C191–18a, the Vicat needle was used to determine the setting time of FA/CFA pastes. The initial and final setting times are described as the durations necessary for the Vicat needle to penetrate 36 ± 1 mm and 0.5 mm, respectively.

2.3.3. Volume stability

Cement pastes of 25 × 25 × 146 mm^3 were prepared for volume stability testing. After curing for 24 hours, the specimen was placed in an automatic autoclave at 215.7℃ with a pressure of 2.0 MPa for 3 hours. The length of the specimen was tested using a specific length meter, and the expansion ratio was calculated using Eq. (1):

$$L_A = \frac{L_1 - L_0}{L} \times 100 \tag{1}$$

where the L_A represents the linear expansion ratio (%); L represents the effective size of the specimen (146 mm); L_0 represents the initial size after demolding (mm); L_1 represents the length after the pressure-steam test (mm).

2.3.4. Hydration heat

The Calmetrix I-CAL 4000 HPC isothermal calorimeter was used to determine the hydration heat of blended pastes at 20°C. Each sample was prepared using 50 g fresh mixture. Water-binder ratios for all mixtures were 0.4. Heat flow was measured every 60 s until 72 h.

2.3.5. Compressive strength

FA/CFA pastes with a size of 40 × 40 × 40 mm^3 were prepared for compressive strength testing, in accordance with ASTM C348.

2.3.6. Nanoindentation

The materials utilized in the nanoindentation testing underwent grinding and polishing to ensure a smooth surface. This polishing process utilizes diamond paste (6 μm, 3 μm, 1 μm, 0.25 μm) applied on a lapping table as specified in [37]. The indentation test was performed using a KLA G200 nanoindenter with a diamond Berkovich tip. To derive the mechanical properties of each phase in the hydrated blended paste, 1200 indentations were carried out on each sample. The load-controlled method was adopted. For each point, the load was linearly increased at a rate of 200 μN/s to a maximum of 2000 μN, sustained for 5 s, and subsequently decreased at the same rate of 200 μN/s [38]. The elastic modulus was derived using the following Eqs. (2)-(4).

$$E_r = \frac{\sqrt{\pi}}{2\beta}\frac{S}{\sqrt{A_c}} \tag{2}$$

$$S = \left(\frac{dP}{dh}\right)_{h=h_{max}} \tag{3}$$

$$\frac{1}{E_r} = \frac{1-\nu^2}{E} + \frac{1-\nu_i^2}{E_i} \tag{4}$$

where β denotes the correlation coefficient of the Berkovich diamond indenter, valued at 1.034; S signifies the contact stiffness, which is determined by P_{max} (maximum load) and h (indentation depth); Ac denotes the contact area; v signifies the Poisson's ratio of the cement sample, which is 0.2. The poisson ratio (0.07) and the elastic modulus (1140 GPa) of the indenter tip are denoted by the symbols E_i and v_i, respectively. The spacing between indents was set as 10 μm to prevent any interaction between adjacent indents. Assuming 4 phases (i.e., outer and inner hydration products, FA particles, unhydrated cement particles) in the matrix and each follows a Gaussian distribution, a deconvolution approach was applied following Ref. [39].

2.3.7. Chemical phases

The hydration of blended paste was terminated at 1, 3, and 28 days, respectively, through a solvent exchange approach using isopropanol. After grounding into power, the sample was dried to a constant weight at 60°C before TG, XRD, and FTIR analyses.

The crystalline structures of FA/CFA pastes were evaluated via XRD using Cu-Kα radiation, scanned within the range of $5° \leq 2\theta \leq 90°$ [40]. FTIR measurement was conducted using the conventional KBr disc method. Frequencies were scanned within the range of 4000–400 cm^{-1}. A Netzsch STA 449F5 thermogravimetric apparatus was used to identify the hydration products of FA/CFA pastes. During the measurement, the samples were heated from 20°C to 900°C while the measurements were performed in a nitrogen atmosphere.

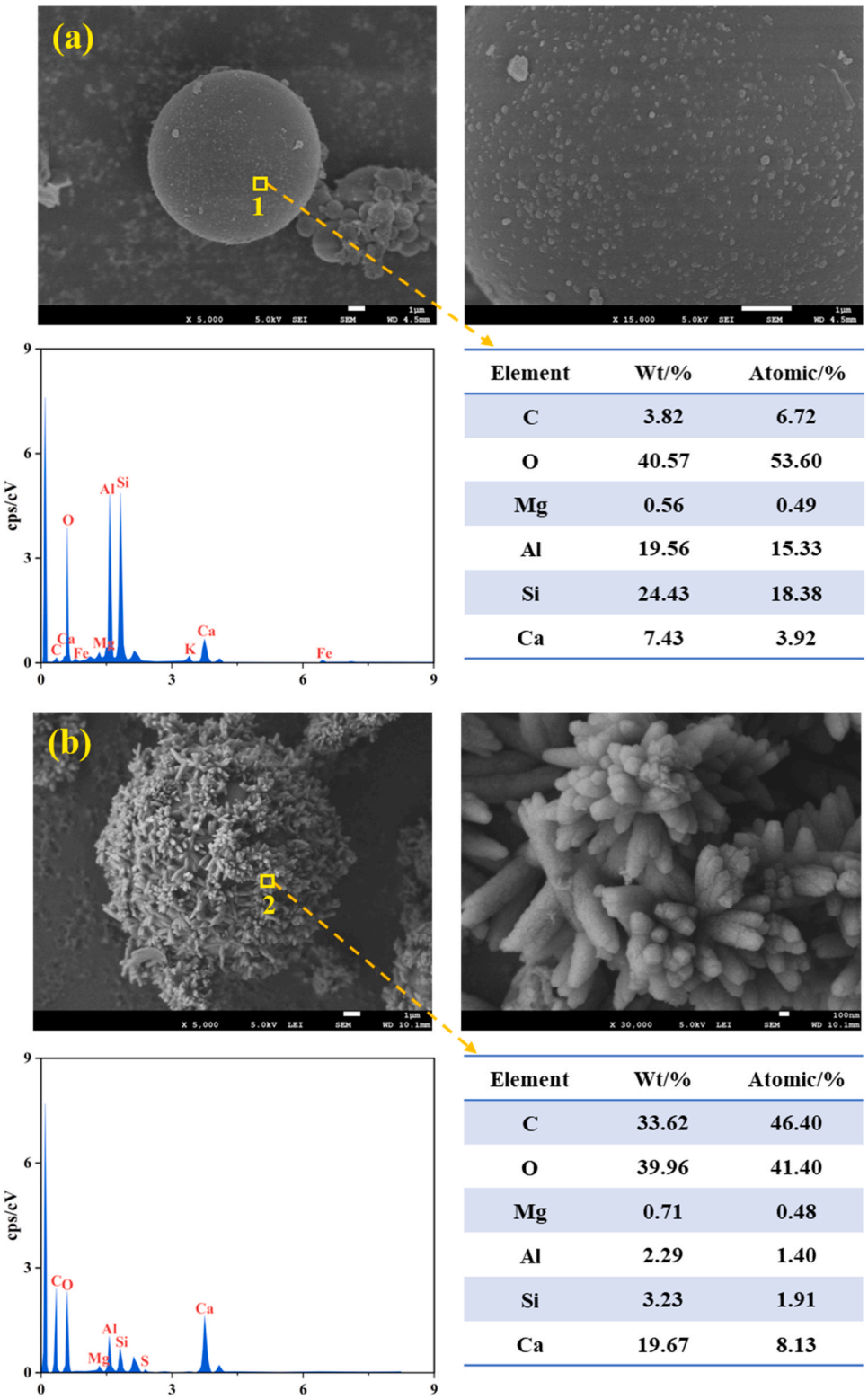

Element	Wt/%	Atomic/%
C	3.82	6.72
O	40.57	53.60
Mg	0.56	0.49
Al	19.56	15.33
Si	24.43	18.38
Ca	7.43	3.92

Element	Wt/%	Atomic/%
C	33.62	46.40
O	39.96	41.40
Mg	0.71	0.48
Al	2.29	1.40
Si	3.23	1.91
Ca	19.67	8.13

Fig. 4. SEM images of carbonated and non-carbonated FA: (a) FA; (b) CFA.

2.3.8. Scanning electronic microscopy-energy dispersive spectroscopy (SEM-EDS)

A JSM-7610F 3 apparatus was used to evaluate the morphology and elemental contents of FA/CFA particles and pastes. Before the test, an ion scattering device was used to apply a thin layer of gold to the samples for 360 seconds.

2.3.9. Mercury intrusion porosimetry (MIP)

The specimen was sectioned following a 28-day curing period and immersed in ethanol for 24 hours to halt hydration. Subsequently, dry in a vacuum oven for 48 hours. An automated mercury porosimeter (Autopore 9220) was used to measure the pore structure of pastes. The measurable pore size range is 3 nm~314 μm, and the measurable pressure range is 4.00×10^{-3}~4.13×10^{-2} MPa.

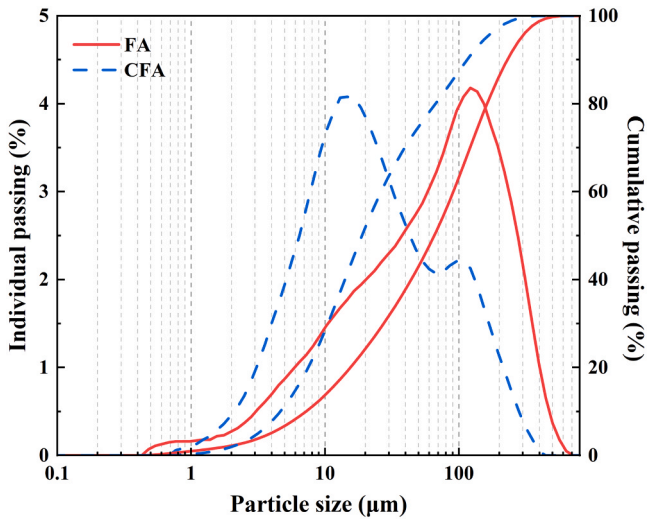

Fig. 5. Particle size distribution of FA before and after carbonation.

Table 3
Specific surface area and particle size distribution of FA and CFA.

Sample	SSA/(m^2/kg)	Particle size distribution (%)		
		< 5 μm	5–20 μm	> 20 μm
FA	144.7	6.73	17.53	75.74
CFA	207.1	11.26	40.63	48.11

3. Results and discussions

3.1. Carbonated FA

3.1.1. Morphology

Fig. 4 illustrates the morphology of FA/CFA. EDS spectra are obtained at the selected spots. From Fig. 4(a), FA is a sphere with some small particles on its surface, since FA may carbonate in the environment, generating small calcite particles. Fig. 4(b) shows the morphology of CFA. The surface of CFA is covered by a large number of calcite crystals. A high-resolution image shows the buildup of fully-grown carbonate crystals. The main morphology of calcite particles on the surface of FA is agglomerated to rod-like. Compared to point 1, the EDS data on point 2 shows a significant increase in C and Ca element content, indicating the formation of $CaCO_3$.

3.1.2. Particle size distribution

FA displays an unimodal particle size distribution [41] and consists of a major population with grain sizes around 100 μm, respectively (Fig. 5). The specific surface area and particle size distribution of FA/CFA are illustrated in Table 3. After carbonation, there is a 43.1 % increase in the specific surface area (SSA). CFA shows a bimodal size distribution. The amount of fine (<5 μm) and medium size (5–20 μm) particles increase, and large (>20 μm) particles decrease. A similar observation has been reported by [42]. The increase of fine particles can be attributed to the aggregation of calcite in the solution. In addition, particle size is reduced due to the leaching of Ca^{2+} and Mg^{2+}. An increase in the volume percentage of medium size is caused by FA surface adsorption and carbonate precipitation. However, different trends are observed for Ref. [23,43] as different carbonation conditions are applied.

3.1.3. Chemical phases and carbonation efficiency

The XRD patterns of original and carbonated FA are compared in Fig. 6(a). There is a significant rise in the diffraction peak intensity of calcite in CFA compared to that in FA. Meanwhile, the portlandite diffraction peaks are significantly attenuated and nearly disappeared. The FTIR results support the XRD findings, as illustrated in Fig. 6(b). The

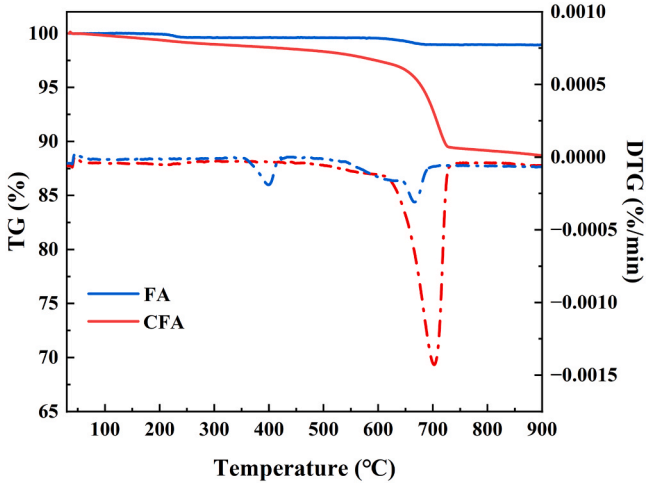

Fig. 7. TG-DTG curves of FA before and after carbonation.

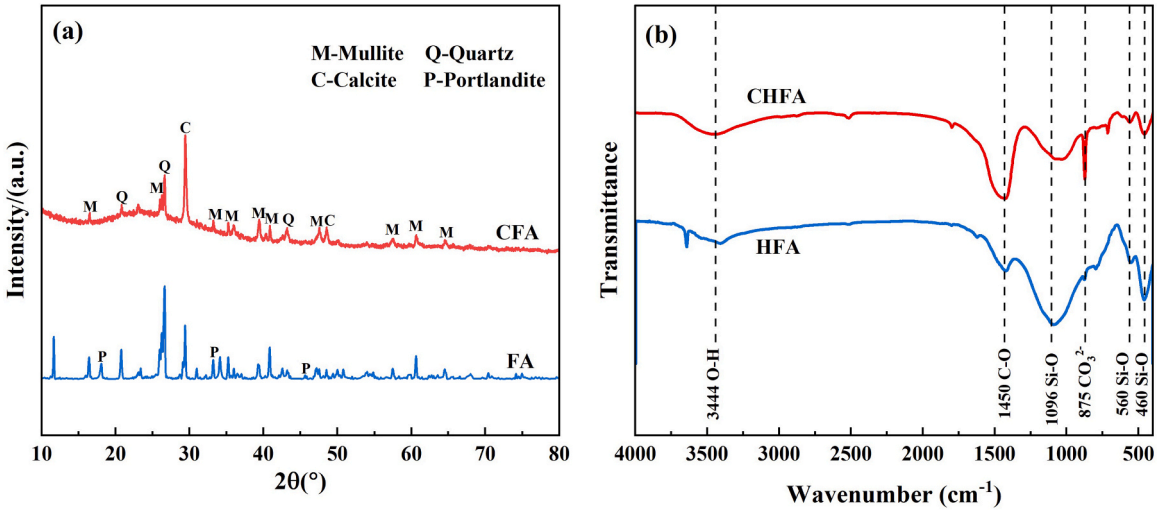

Fig. 6. XRD and FTIR results of FA/CFA: (a) XRD; (b) FTIR.

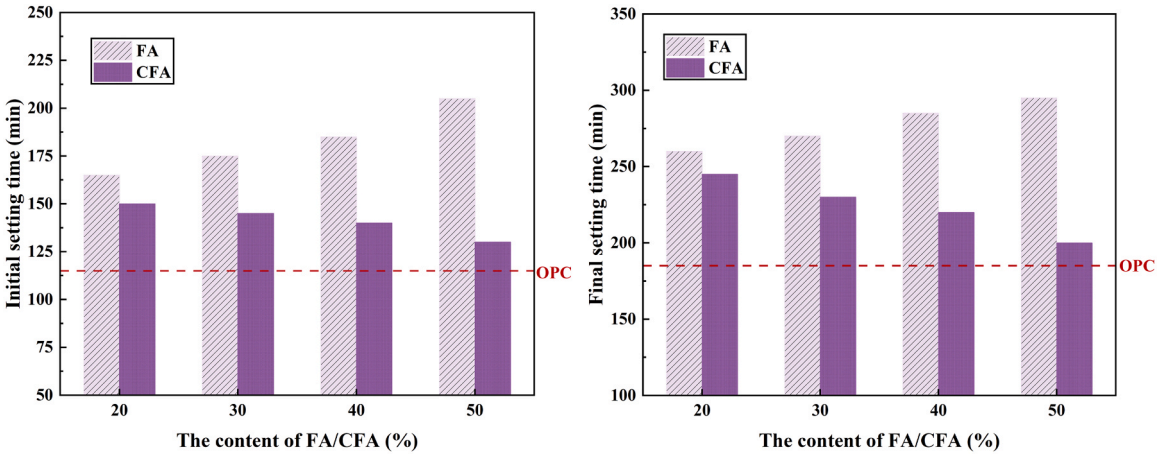

Fig. 8. The initial and final setting time of FA/CFA pastes.

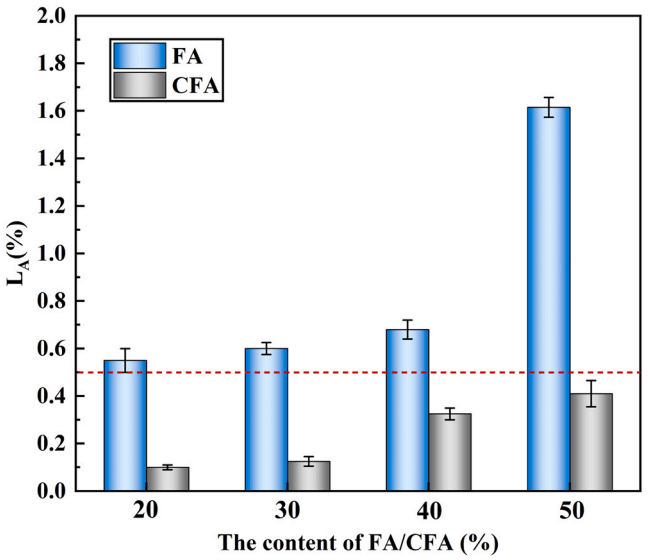

Fig. 9. Volumetric stability of FA/CFA pastes.

peaks at 460 cm^{-1}, 560 cm^{-1}, and 1096 cm^{-1}, seen in all FA particles, indicate Si-O stretching vibrations, implying the presence of quartz. In FA, there is a prominent absorption band at 3444 cm^{-1}, suggesting the existence of O-H from water molecules [44]. The CO_3^{2-} bending (ν_2, 875 cm^{-1}) band and C-O bending (ν_3, 1420 cm^{-1}) are attributed to the peak characteristic of calcite [45]. An extra absorption band is present at 1793–1799 cm^{-1} for CFA particles, indicating the presence of calcite. In addition, the absorption band at 745 cm^{-1} indicates the existence of vaterite, which is undetectable by XRD due to its low concentration. Unlike the carbonation system using hydrated cement paste powder or steel slag [46–48], no silica gel or calcium silicate mineral is generated during the carbonation process using FA. This is due to the slow hydration process of FA [49,50], and the carbonation process lasts only 6 minutes, limiting the production of silica gel and calcium silicate minerals.

TG-DTG results are presented in Fig. 7. A significant loss of mass in FA occurs between 380°C and 430°C, referred to the decomposition of portlandite [51]. The mass loss peak at 550–900℃ represented the decomposition of calcite [52], consistent with the observations in XRD and FTIR. The CO_2 uptake and the amount of calcite can be calculated based on TG-DTG results, as follows in Eqs. (5)-(7) [53]:

$$w(CO_2)\left(wt\%\right) = \frac{\Delta m_{550-900^{\circ}C}}{m_0} \times 100 \tag{5}$$

$$CO_{2\text{uptake}}\left(\text{wt\%}\right) = \frac{w(CO_2)(wt\%)}{100 - w(CO_2)(wt\%)} \times 100 \tag{6}$$

$$M_{CaCO_3}\left(\text{wt\%}\right) = \frac{\Delta m_{550-900^{\circ}C}}{m_0} \times \frac{100}{44} \times 100 \tag{7}$$

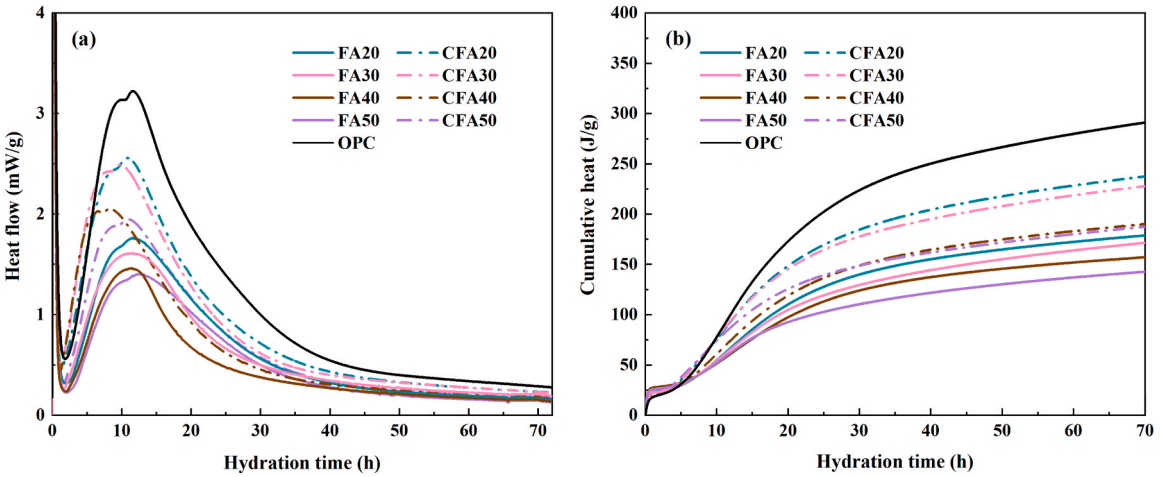

Fig. 10. Hydration heat of FA/CFA pastes: (a) heat flow curves; (b) cumulative heat.

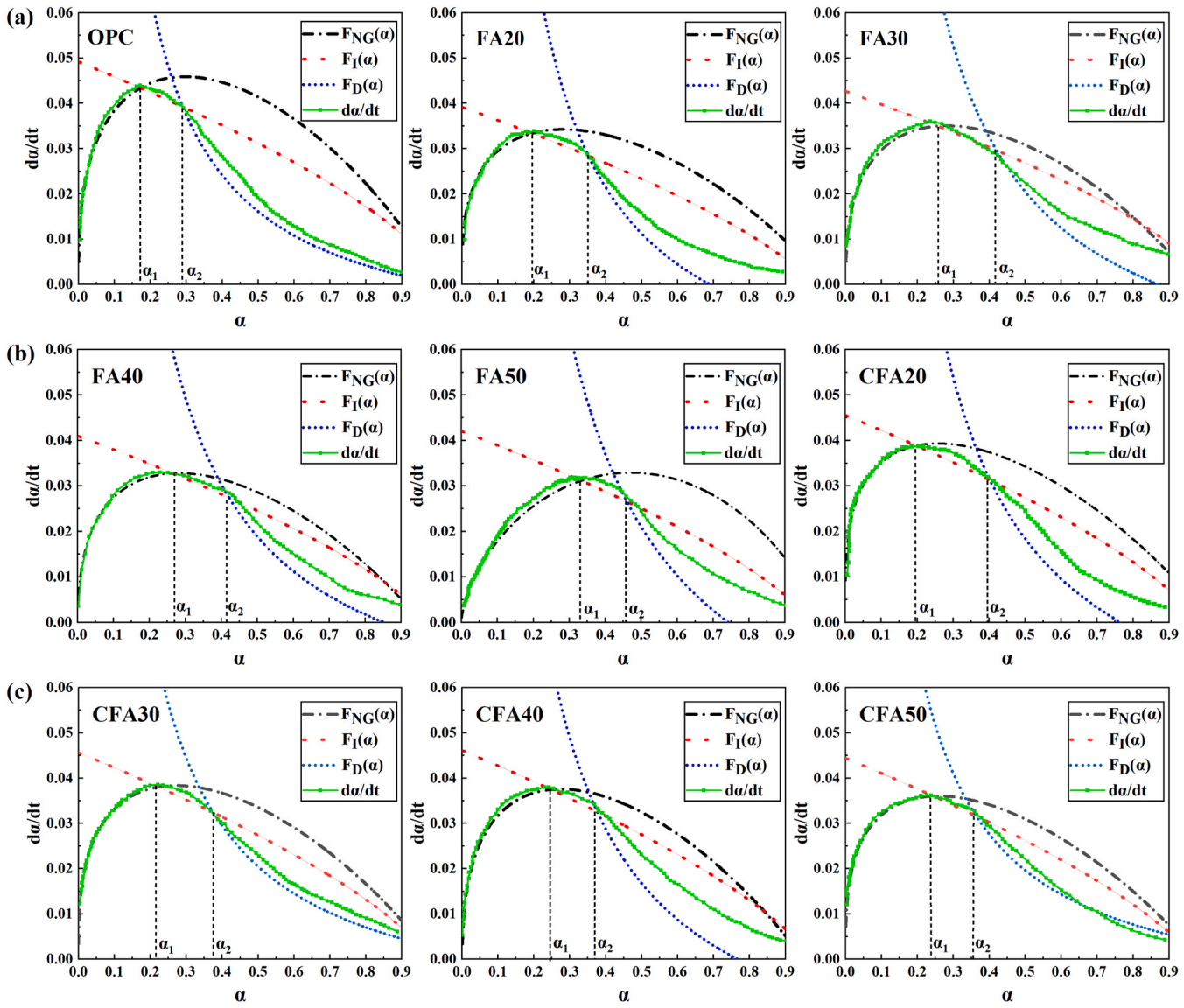

Fig. 11. The correlation among FNG(α), FI(α), and FD(α) with the degree of hydration (α).

Table 4
Kinetic parameters of the paste samples.

Sample	n	K'$_{NG}$	K'$_{I}$	K'$_{D}$	Hydration mechanism	α_1	α_2	α_2-α_1
OPC	1.56421	0.06024	0.01619	0.00594	NG-I-D	0.1738	0.2919	0.1181
FA20	1.48658	0.05745	0.01413	0.00562		0.1859	0.3487	0.1628
FA30	1.49241	0.05110	0.01427	0.00538		0.2574	0.4169	0.1595
FA40	1.49652	0.05062	0.01486	0.00512		0.2686	0.4150	0.1464
FA50	1.50210	0.05018	0.01534	0.00501		0.3305	0.4591	0.1286
CFA20	1.48021	0.06005	0.01572	0.00468		0.1940	0.3953	0.2013
CFA30	1.47516	0.05906	0.01679	0.00456		0.2203	0.3830	0.1627
CFA40	1.46523	0.05432	0.01645	0.00401		0.2377	0.3713	0.1336
CFA50	1.42534	0.05263	0.01637	0.00357		0.2301	0.3502	0.1201

where Δm550–900℃ is the weight loss between 550 and 900℃, m_0 represents the starting mass of the samples, whereas w (CO_2) denotes the mass percentage of CO_2; M_{CaCO_3} is the amount of $CaCO_3$. The molecular weights of CO_2, Ca, and CaO are MW_{CO_2}, MW_{Ca}, and MW_{CaO} (g/mol). The carbonation efficiency (ζCaO) of FA is determined by Eq. (8):

$$\zeta CaO(\%) = \frac{\frac{w(CO_2)}{100-w(CO_2)} \times \frac{1}{MW_{CO_2}}}{Ca_{total}/MW_{Ca}} = \frac{\frac{w(CO_2)}{100-w(CO_2)} \times \frac{1}{MW_{CO_2}}}{CaO_{total}/MW_{CaO}} \quad (8)$$

where Ca_{total} and CaO_{total} represent the weight percent fractions ascertained using XRF analysis.

CFA achieves a CO_2 uptake of 94 kg/t and carbonation efficiency of 59.82 %, higher than the data reported in the literature in which acid/salt and other extractants are used. As reported by [54–56], carbon sequestration of class C FA (w_{CaO}>20 %) is less than 86 kg/t. This number decreases to 17.36 kg/t when class F FA is used [57].

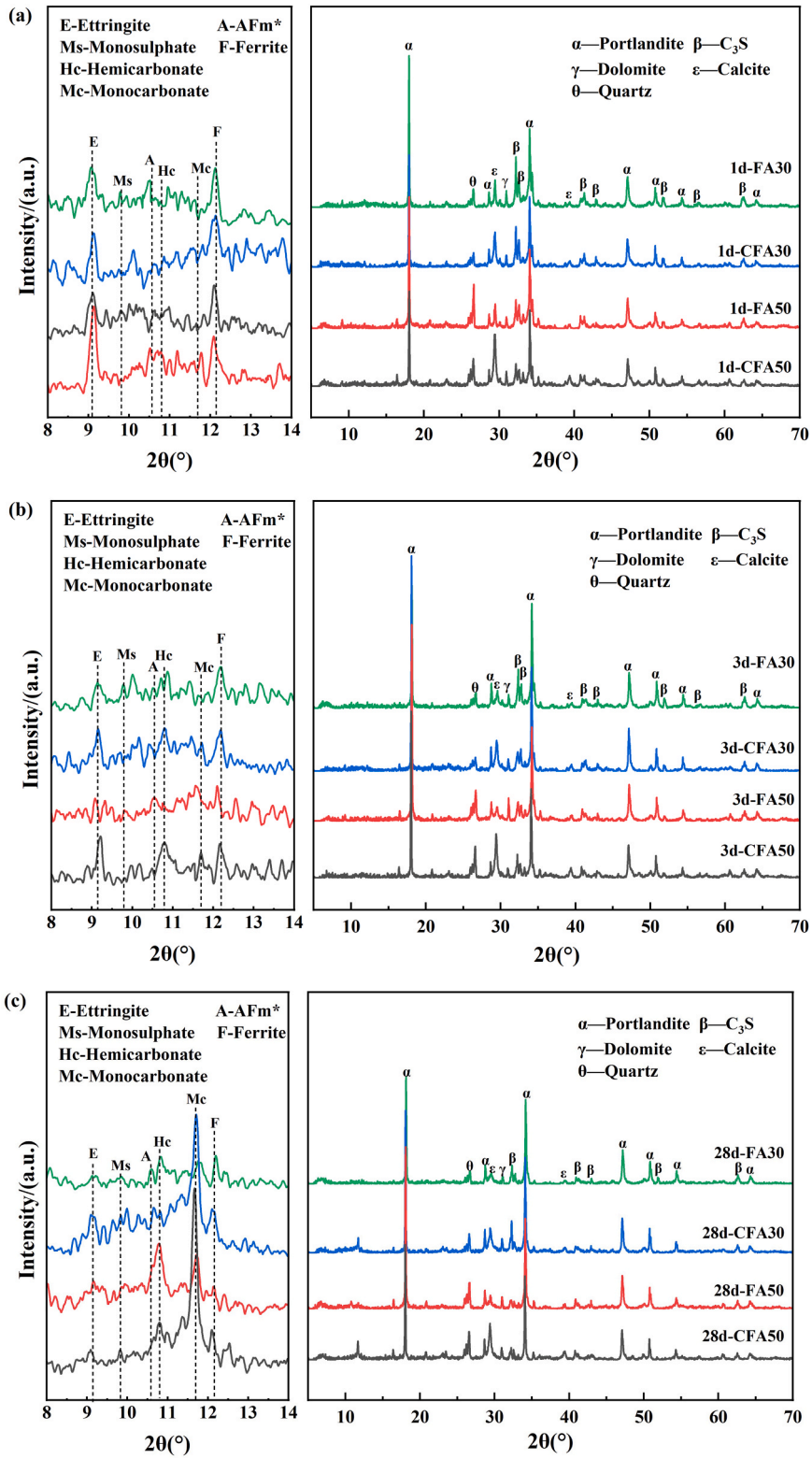

Fig. 12. XRD patterns of FA/CFA pastes at different ages: (a) 1 day; (b) 3 days; (c) 28 days.

3.2. Blended OPC-FA/CFA pastes

3.2.1. Setting Time

Fig. 8 shows the initial and final setting time of FA/CFA pastes. As expected, the addition of FA in cement significantly delays the setting. This is because FA particles mainly work as a diluent material at early ages, not participating during the flocculation and setting processes [58]. The carbonation treatment can effectively improve the retarding phenomenon of FA paste. From Fig. 8, the initial and final setting time of CFA 30 are 17.14 % and 14.81 % faster than that of FA30. The initial and final setting times decrease as the CFA content rises. Nano-sized calcite particles attached to the CFA can serve as nucleation sites for the precipitation and development of C-S-H gel and other hydrates. Ca^{2+} can be rapidly adsorbed in the pore fluid, reducing Ca^{2+} concentrations

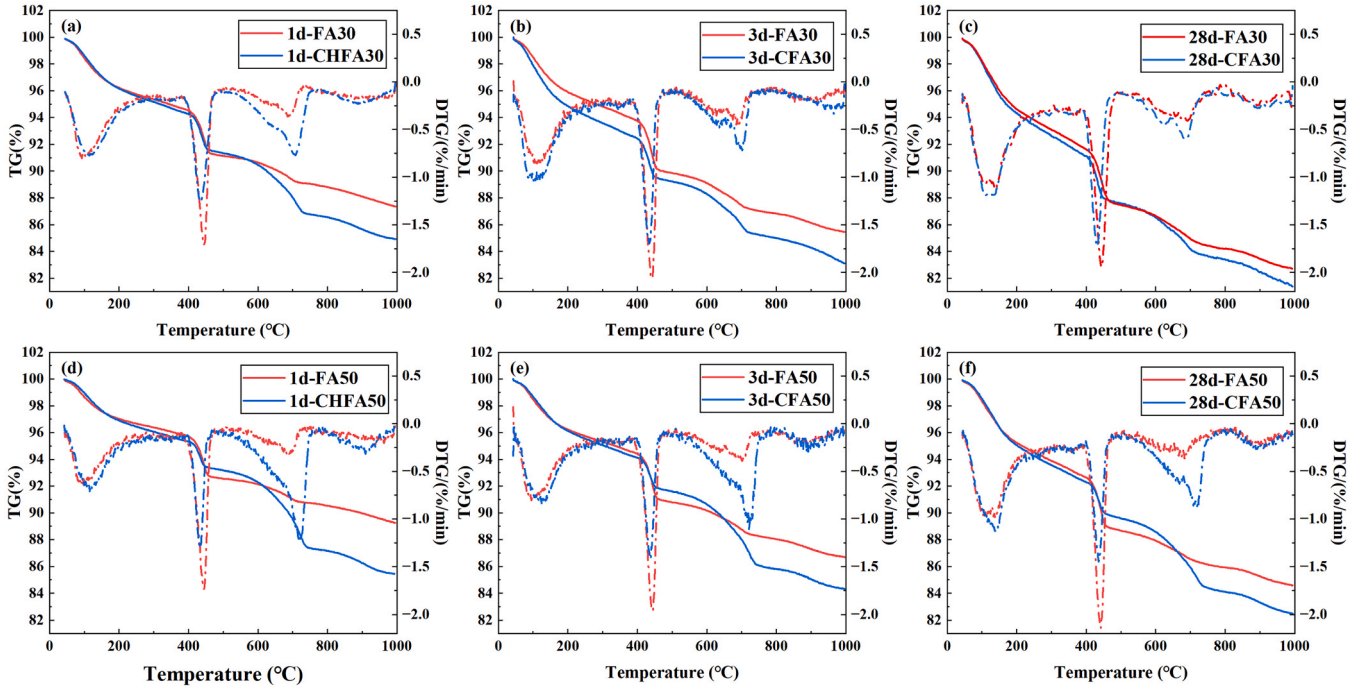

Fig. 13. TG-DTG analysis of FA/CFA pastes at different ages.

Table 5
Content of hydrate water and portlandite in cement paste.

Age (day)	Mixes	Hydrate water (wt%)	CH (wt%)	$CaCO_3$ (wt%)
1 day	FA30	9.82	16.53	2.14
	CFA30	9.93	15.17	4.47
	FA50	7.68	15.05	1.88
	CFA50	7.68	11.55	5.71
3 days	FA30	11.52	19.49	2.75
	CFA30	12.39	16.86	3.90
	FA50	9.53	17.84	2.52
	CFA50	10.40	13.73	5.47
28 days	FA30	14.48	21.87	3.0
	CFA30	14.70	19.61	3.76
	FA50	12.03	20.23	2.43
	CFA50	13.12	15.25	5.13

around C_3S and further accelerating C_3S hydration [59]. As a result, the early hydration reaction for C-S-H gel formation is accelerated, and the setting time is reduced [60,61].

3.2.2. *Volume stability*

Fig. 9 shows the linear expansion ratio (L_A/%) after 3 hours of steaming in the autoclave. The expansion ratio increases with class C FA content. With the content of FA increases from 20 % to 50 %, the L_A of FA blended paste grows from 0.55 % to 1.62 %, exceeding 0.5 %. This means that the volume stability of FA pastes does not meet the specification requirements. The f-CaO in class C FA leads to the expansion. The volume stability of FA is improved after carbonation pre-treatment, and the expansion ratio of blended paste incorporation of 20 %-50 % CFA is between 0.1 % and 0.41 % (<0.5 %). This means the carbonation treatment can effectively improve the volume stability of class C FA. The main reason is that carbonation consumes f-CaO in FA pastes. The f-CaO content of class C FA is 5.51 %, but it is below 0.01 % in CFA. A threshold for expansion occurs when the percentage of FA is 50 %. The reasons can be summarized as follows. Firstly, the f-CaO content in OPC-FA system increases with FA dosage increasing and produces larger crystallization pressure during hydration. Secondly, as FA content increases, mechanical properties of the paste are hindered, which reduces the resistance ability to deformation and crack.

3.2.3. *Hydration kinetics*

The measured hydration heat for FA/CFA pastes is shown in Fig. 10, and the heat flow results are normalized per gram of binder. The addition of FA plays a role in diluting cement in the early stage of hydration, which reduces the total hydration heat [62,63].

From Fig. 10 (a), the main hydration peak consists of two humps. The first peak arises from the hydration of calcium silicates, particularly C_3S. The substitution of FA with CFA leads to an increased intensity of the first peak, indicating that CFA enhances the dissolution of ions [64]. The second peak corresponds to the further hydration of tricalcium aluminate (C_3A) [65]. The accelerated aluminate reaction may be linked to the generation of mono-carboaluminate (Mc) and hemi-carboaluminate (Hc) from the dissolved carbonate ions, as reported by previous studies [66,67]. According to 11(b), the replacement of OPC by FA results in a reduction of the total heat. Compared with FA, CFA can promote the hydration process. Specifically, the cumulative heat of CFA20、CFA30、CFA40、CFA50 are increased by 32.29 %、21.94 %、33.58.27 %、34.01 % compared with FA20、FA30、FA40 and FA50, respectively.

The Krstulovic-Dabic model can be used to simulate cement hydration. According to references [68,69], the parameters of Krstulovic-Dabic model are calculated. The theoretical hydration curves of FA/CFA pastes are shown in Fig. 11. OPC-FA/CFA system undergoes three phases: nucleation and crystal growth (NG), phase boundary reaction (I), and diffusion (D) [69]. The Kinetic parameters of the paste samples are shown in Table 4. Compared with pure OPC, adding FA/CFA reduces the reaction rate in each hydration stage. The value of reaction steps (n) in the CFA paste decreases, and the reaction rate constant (K'_{NG}) increases during the control stage of NG process. The decrease of n indicates that the reaction complexity increases, while the increase of K'_{NG} indicates that the reaction is promoted [70]. It is found that CFA pastes have a higher K'_I value than FA pastes with the same replacement ratio, which means the carbonation treatment increases the NG process. In the control stage of I process, the reaction rate constant K'_I of CFA pastes is higher than FA pastes, indicating that the CFA hydration rate is accelerated in the I process.

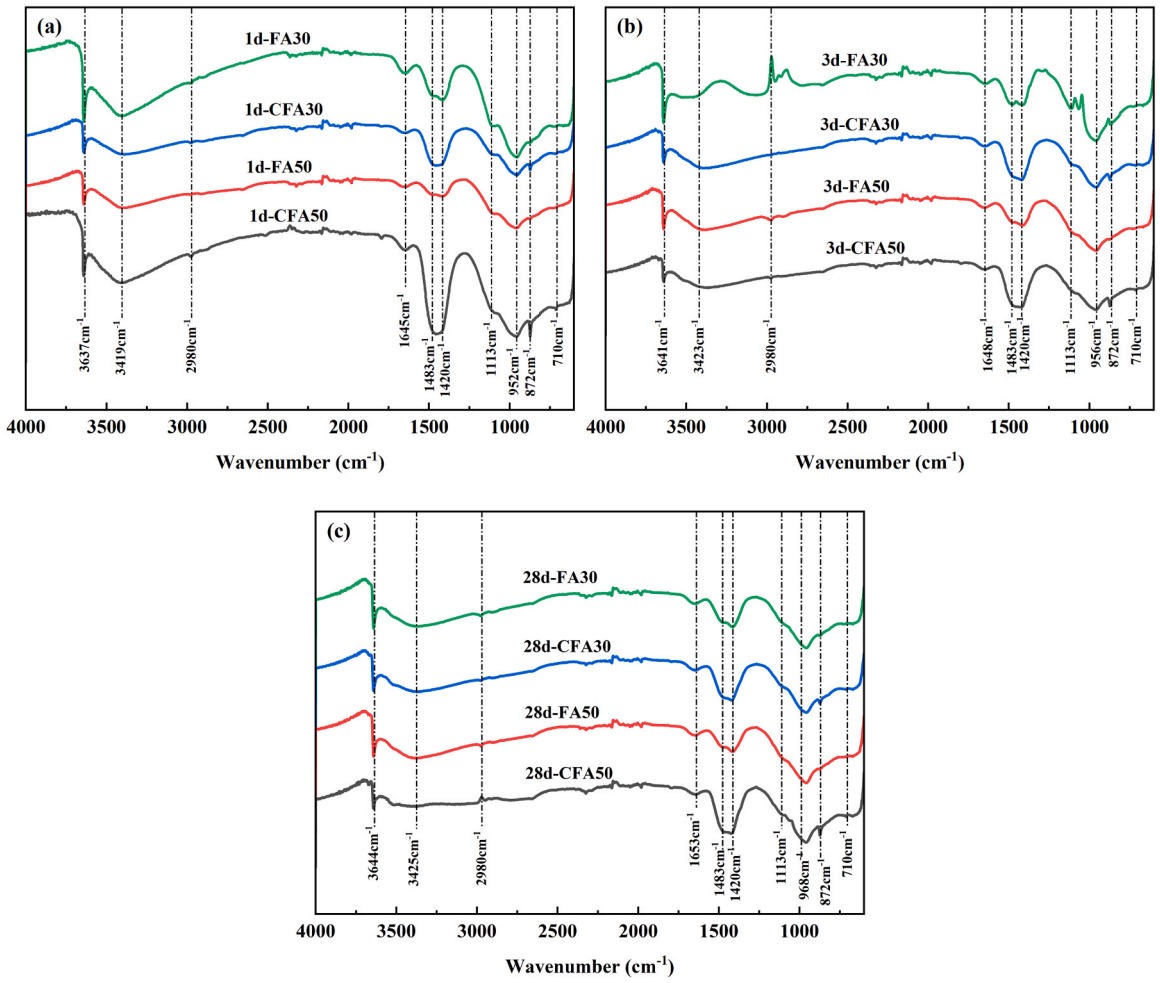

Fig. 14. FTIR spectra of FA/CFA pastes at different ages: (a) 1 day; (b) 3 days; (c) 28 days.

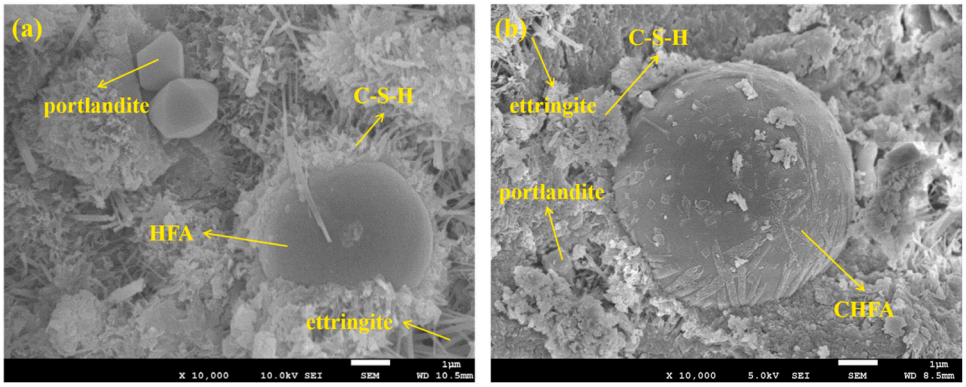

Fig. 15. SEM images of cement pastes after 3 days of hydration: (a) FA30; (b) CFA30.

Plenty of hydration products are wrapped around particles during the later stage of hydration. Thus, the product layer inhibits Ca^{2+} leaching at a later stage. The hydration reaction is controlled by a diffusion process, which corresponds to D process. For FA/CFA pastes, K'_D decreased significantly compared with K'_I of I process, indicating a rapid decline in hydration rate. Although nano-sized calcite can enhance the growth of C-S-H in NG process, it may adversely affect D processes [70]. A denser product layer forms around the cement clinker, impeding the transportation of moisture and ions. Thus, CFA pastes exhibit a lower K'_D than FA pastes. Table 4 illustrates that the crossovers with the respective hydration degrees α_1 and α_2 signify the transition locations from NG to I and from I to D. The difference between α_1 and α_2 reflects the degree of phase boundary reaction, which depends on the barrier of ion migration and is influenced by the amount of hydration products [68,71]. The reduction of the difference means that nano-sized calcite accelerates the hydration degree from NG to I process.

3.2.4. *Hydration products characterization*

3.2.4.1. Crystalline phase compositions. Fig. 12 shows a comparison of

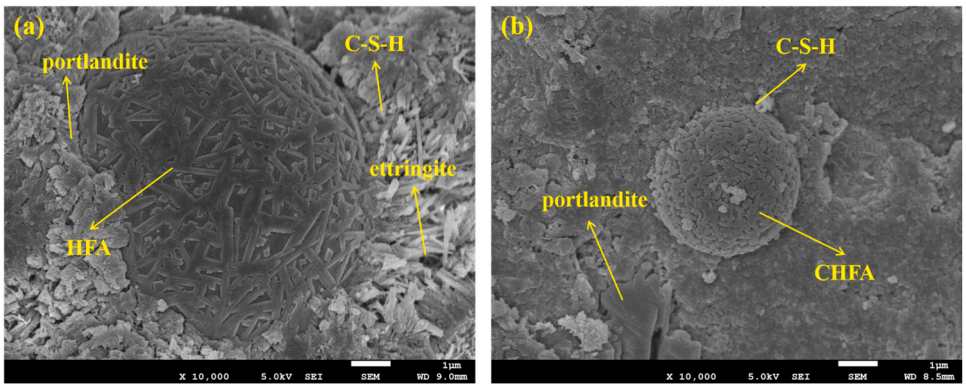

Fig. 16. SEM images of cement pastes after 28 days of hydration: (a) FA30; (b) CFA30.

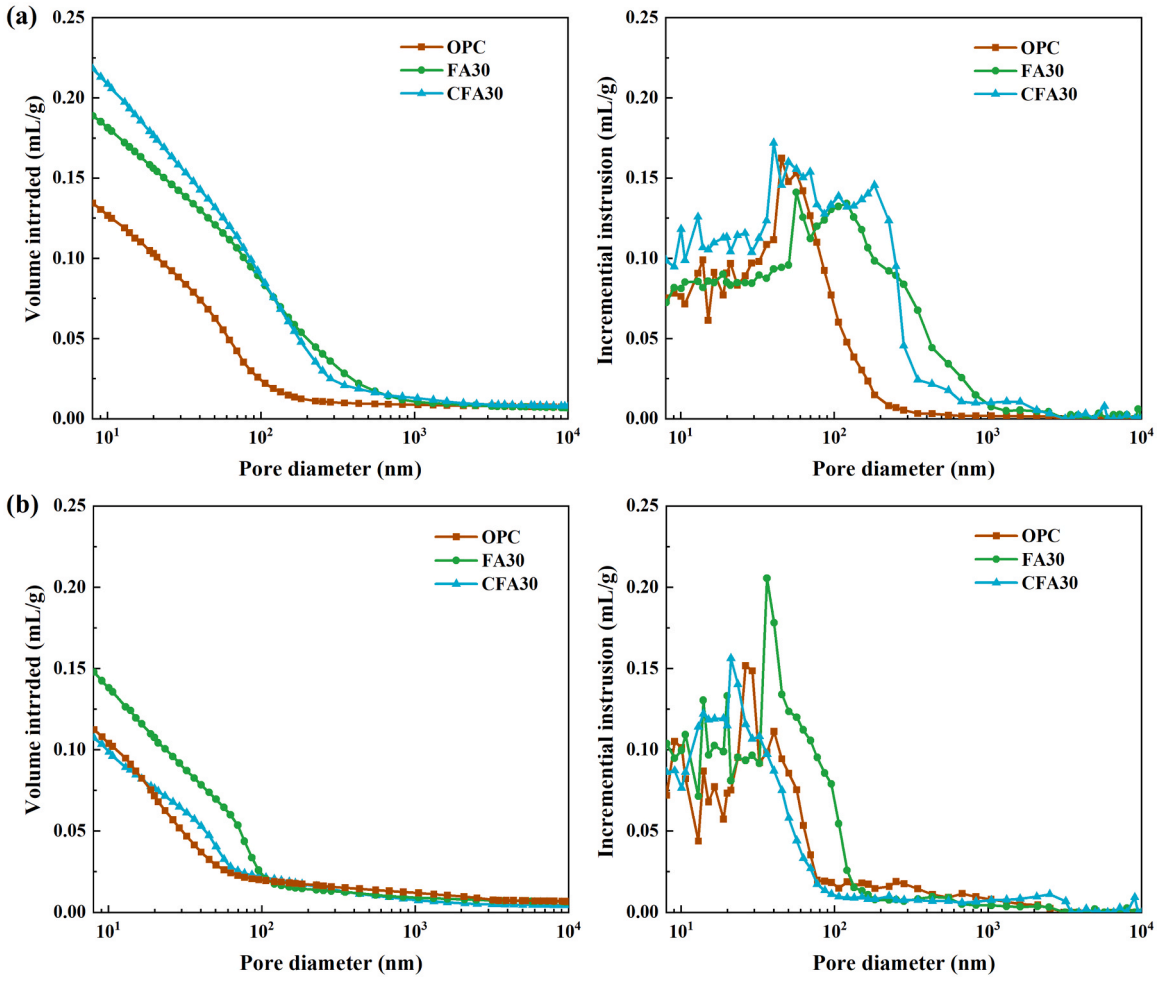

Fig. 17. MIP results with FA30 and CFA30: (a) 3 days; (b) 28 days.

the XRD patterns of the hydrated cement pastes at low angles. At 1 day, C_3A interacts with gypsum to produce ettringite. (AFt 9.1° 2θ). Once gypsum is depleted, the remaining aluminates react with AFt to form monosulfate (Ms 9.8° 2θ). In CFA pastes, the attached calcite reacts with aluminates to produce Mc (11.7° 2θ) and Hc (10.8° 2θ). In this process, the conversion from AFt to Ms is inhibited; therefore, the amount of Ms in CFA pastes is much lower than in FA pastes.

At 3 days, more AFt is retained in CFA paste, consistent with references [72,73] where $CaCO_3$ particles are applied in OPC-FA system. The higher the CFA replacement ratio, the higher the AFt content remains. As the curing age increases, AFt gradually participates in the reaction, and its content decreases. The contents of Hc and Mc increased gradually with the increase of curing age, exhibiting minimal difference between Hc and Mc. In addition, for OPC-FA system, there is also a broad peak between Ms and Hc, which may be related to the carbonate and sulfate containing hydroxy-AFm (AFm*) [74]. At 28 days, AFm* remains in OPC-FA system, the reduction of ettringite and increase of Ms in OPC/FA and OPC/CFA is observed due to the on-going hydration. Furthermore, Hc peak decreases in CFA pastes, whereas the peak of Mc increases with time. This may be due to Mc is thermodynamically more stable than Hc

Table 6
Pore structure parameters of FA30 and CFA30.

Samples	Age (day)	Porosity (%)	Unit mercury intake (mL/g)	Threshold pore diameter (nm)
OPC	3	25.31	0.15	43.57
FA30		33.60	0.23	52.16
CFA30		30.53	0.20	38.99
OPC	28	20.86	0.12	26.39
FA30		25.55	0.16	38.26
CFA30		22.07	0.13	21.91

[75,76]. FA50 also contains a large amount of Hc and Mc, and it can be deduced that the carbonate is generated through natural carbonation due to the presence of CaO in Class C FA. The ferrite content (12.2° 2θ) diminishes as the curing age increases.

3.2.4.2. TG-DTG analysis. Fig. 13 shows the TG-DTG curves of hydrated cement pastes. The hydration product is related to the decomposition of carbonate, which can be used to determine the hydration degree. Generally, the greater the weight loss of the hydrated paste, the higher its hydration degree. The weight loss ($W_{C\text{-}S\text{-}H}$) at 30–200°C corresponds to the decomposition of AFt, monosulfate, and C-S-H gel [77]. The weight loss (W_{CH}) between 350°C and 500°C is attributed to the decomposition of portlandite [51]. The weight loss (W_{CaCO3}) between 550°C and 900°C corresponds to the decomposition of calcite [52,78,79]. The hydrate water content (W_H) and CH mass content (W_{CH}) are calculated in the hydrated blended cement paste (Eqs. (9)-(10)):

$$H = \frac{\Delta m_{40-500^\circ C}}{m_{500^\circ C}} \tag{9}$$

$$CH = \frac{\Delta m_{350-500^\circ C}}{m_0} \times \frac{74}{18} \tag{10}$$

where $\Delta m_{40–500℃}$ is the weight loss between 40 and 500℃, m_0 is the initial mass, $\Delta m_{350–500℃}$ is the weight loss between 350 and 500℃.

The calculated hydrate water, as well as CH content in FA/CFA pastes, are shown in Table 5. With FA/CFA content increasing, hydrate water in pastes decreases gradually, indicating fewer hydration products. CFA pastes contain more hydrated water than FA pastes at the same replacement level, promoting the hydration process. As the FA/CFA dosage increases, the CH content decreases gradually. Furthermore, the CH content in the FA/CFA pastes increases gradually as the hydration age increases because FA/CFA pozzolanic reactions are much slower than cement clinker hydration. The CH content of CFA paste is significantly lower than that of FA paste, primarily because the carbonation treatment consumes CH in the FA. Moreover, CH participates in the reaction between aluminates and calcite [80]. This also leads to the reduction of calcite as hydration proceeds.

3.2.4.3. FTIR. FTIR spectrum is shown in Fig. 14. The intensity of peaks and their relative displacement are closely associated with molecular groups and hydration products. The shoulder peak at 3642 cm^{-1} is attributed to the hydroxyl group in $Ca(OH)_2$. As curing age increases, the band shifts to a high wavenumber, which indicates an increase in CH [81,82]. The H_2O (O-H) bends at 3444 cm^{-1} and 1640 cm^{-1} slightly shift to high wavenumbers, indicating the gradual conversion of interlayer water to bound water and the formation of C-S-H [83]. The leftward shift of the Si-O-Si band peak near 970 cm^{-1} suggests an increase of C-S-H gel. The peak near 3640 cm^{-1} corresponds to hydroxyl groups and the -OH in $Ca(OH)_2$, and the shoulder band shifts slightly toward higher wavenumbers with the increase of curing time, indicating an increase in CH [81–83]. Moreover, vibrational peaks of CO_3^{2-} at 1421 cm^{-1} and 875 cm^{-1} are indicative of calcium carbonate [84]. The vibrational peaks rise significantly with increased CFA content, suggesting that calcite can be formed in large quantities after carbonation. Calcite content increases sequentially with the dosage of CFA paste. The peak gradually stabilized at 28 days, which suggests that calcite is consumed. This is consistent with XRD and TG results.

3.2.5. Microstructure evolution

3.2.5.1. Morphology of microstructures. The SEM images of cement pastes containing 30 % FA and CFA at 3- and 28 days are shown in Figs. 15- 16, respectively. FA plays a role in filling and mainly acts as a micro-aggregate. C-S-H gel and CH are visible. With hydration time going on, hydration products accumulate on FA particles. FA particles become honeycomb due to pozzolanic reactions [85,86].

The hardened FA and CFA pastes at 28 days exhibit considerably greater density compared to 3 days. As the hydration process progresses, hydration products accumulate on FA particles. After 28 days, a large amount of densified hydration products is observed. Furthermore, FA is encapsulated by C-S-H gel since the CH around the FA is consumed rather than retained [83,87,88]. More severe dissolution is also observed on the CFA surface, indicating a higher degree of reaction. However, some FA particles retained a smooth texture, suggesting that these particles partially served as inert materials to enhance the packing density of the cementitious matrix [89,90].

3.2.5.2. Pore structure. Fig. 17 illustrates the pore size distribution of

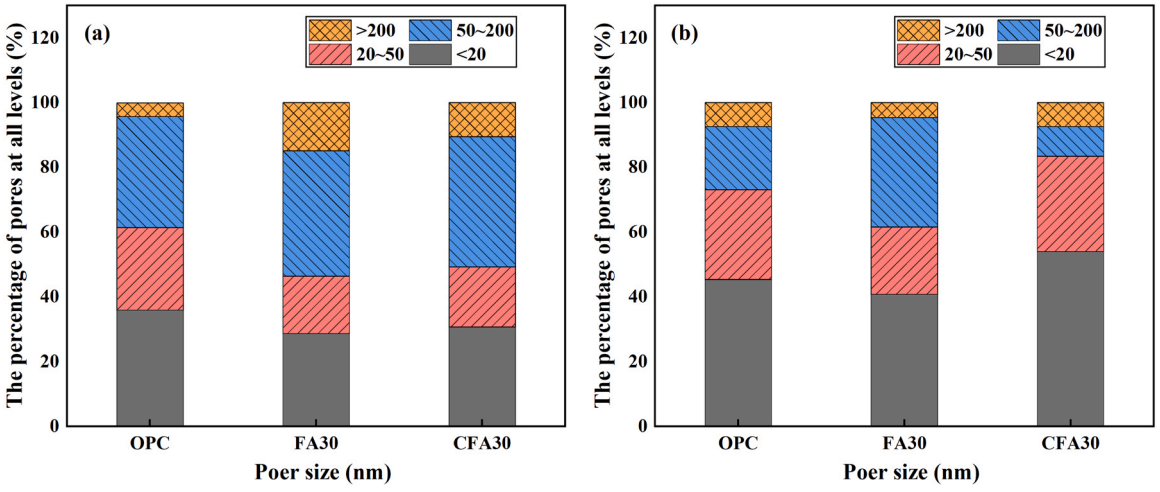

Fig. 18. Pore diameter distribution of FA/CFA pastes: (a) 3 days; (b) 28 days.

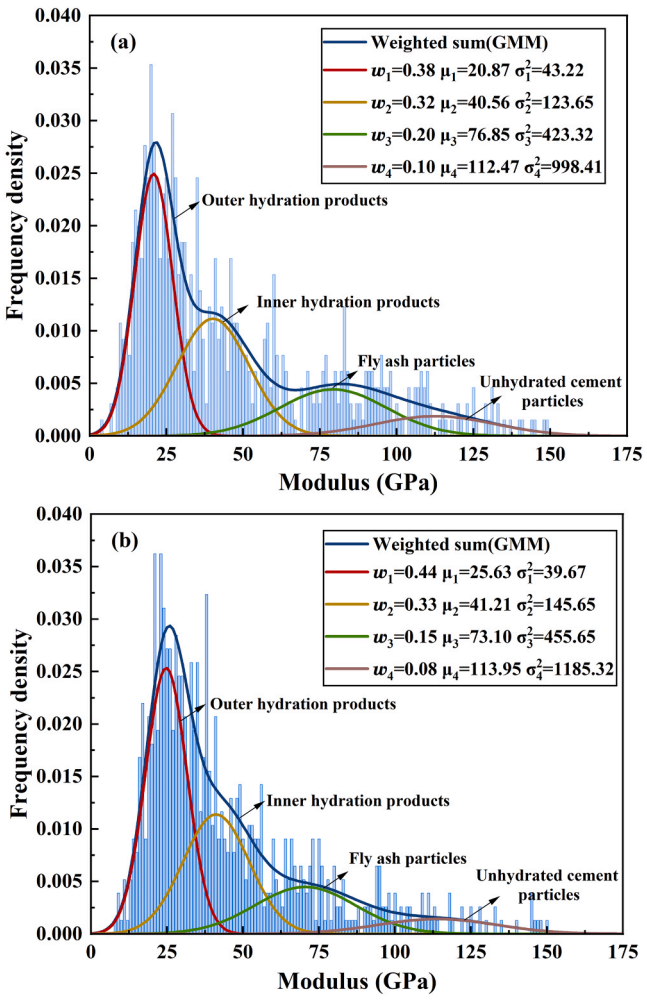

Fig. 19. Gaussian distribution fitting results: (a) FA30; (b) CFA30.

FA30 and CFA30 at 3 and 28 days, respectively. Porosity and threshold pore diameter are calculated and shown in Table 6. At 3 days, OPC exhibits the lowest porosity, whereas FA30 has the highest porosity, and the porosity of CFA30 is 9.14 % lower than that of FA30. The threshold pore diameter of CFA30 is 25.2 % smaller than that of FA30. With curing time going on, CFA has a more significant effect on refining the pore size. Compared with FA30, the porosity and threshold pore diameter of CFA30 at 28 days decreased by 13.6 % and 42.7 %, respectively.

Based on Ref [91], pore sizes can be categorized into four types: harmless pores (<20 nm), less harmful pores (20–50 nm), harmful pores (50–200 nm), and multi-harmful pores (> 200 nm). As shown in Fig. 18, the proportion of harmless, less harmful, and harmful pores in CFA30 show a slight change compared with FA30 at 3 days, while the volume proportion of multi-harmful pores decreases by 29.5 %. At 28 days, the proportion of multi-harmful pores in FA and CFA pastes decreased by 69.1 % and 29.5 % compared with 3 days, respectively. Compared with FA30, the proportion of harmful pores in CFA30 decreases by 72.8 %. CFA can transform harmful and multi-harmful pores into less harmful or harmless pores.

3.2.6. *Micromechanical properties*

Fig. 19 shows the frequency distribution of the measured elastic modulus using nanoindentation. Phases with high elastic modulus (greater than 90 GPa) correspond to unhydrated cement particles [39], and phases with elastic modulus between 70 and 80 GPa correspond to FA particles. The hydration products can be classified as outer hydration products with elastic modulus between 20 and 30 GPa and inner hydration products with elastic modulus between 35 and 45 GPa.

Compared with FA paste, the average elastic modulus of outer hydration products in CFA pastes increases by 5 MPa. This supports the hydration kinetics model in Section 3.2.3, as a denser hydration product layer generally corresponds to more excellent mechanical properties. Furthermore, CFA paste has 15.8 % more outer hydration products than FA paste. The reasons can be summarized as follows. Firstly, calcite in CFA is involved in the hydration process; calcite can provide active nucleation sites for hydrates, which can effectively promote the crystallization and precipitation of C-S-H [92]. Secondly, calcite participates in the formation of Mc and Hc and reserves AFt in the matrix, which has a higher density and elastic modulus than AFm Phase. Moreover, calcite and outer hydration products have similar elastic modulus; some might be calcite. The formation of inner hydration products occurs within the clinker, resulting in no variation in the percentage or strength of inner hydration products between FA and CFA pastes.

3.2.7. *Compressive strength development*

Fig. 20 shows the compressive strength of FA/CFA pastes. The compressive strength of FA pastes shows a decreasing trend as substitution ratios increase. Compared with FA pastes, the 28-day compressive strength of CFA pastes increases by 28.3 %, 30.07 %, 40.29 %, and 55.94 % at a replacement level of 20 %, 30 %, 40 %, and 50 %, respectively. The improvement in strength is more remarkable at a higher replacement level. The incorporation of CFA has a more pronounced impact on compressive strength at an early age than at 28 days. Compared to FA50, CFA50 exhibits 98.97 % and 113.41 % higher compressive strengths at 1 and 3 days, respectively. The compressive strength of per kilogram cement is calculated and shown in Table 7. FA significantly reduces the compressive strength of per kilogram cement. CFA pastes have a greater unit strength than FA pastes, indicating that carbonation can improve the reactivity of FA. The unit strength of CFA pastes is comparable to or even exceeds the value of OPC when CFA dosage is 20 %-40 %, indicating that CFA contributes to the strength in the hydration process.

The early strength improvement achieved by carbonationcan be attributed to the following factors. $CaCO_3$ particles in CFA can provide active nucleation sites for hydrates and contribute to the formation of Mc and Hc. Ettringite is preserved in this process, with a greater volume than Ms and AFm [93]. Additionally, CFA may improve the amount and density of outer hydration products. Consequently, harmful and multi-detrimental pores are converted into less harmful or harmless pores, resulting in an improved pore structure.

4. Conclusions

In this paper, high-calcium content FA was carbonated by direct wet method and used as SCMs. The impact of CFA content on the initial volume stability, mechanical characteristics, and hydration mechanisms of cement paste was investigated. The following conclusions can be obtained.

(1) The carbonation product on the surface of FA particles is calcite. The particle size distribution curve of CFA is shifted to the smaller side compared with FA and concentrates in the range of 5–20 μm. The carbonation procedure achieves a CO_2 uptake of 94 kg/t and a carbonation efficiency of 59.82 %, higher than the data reported in the literature.

(2) CFA can improve the strength of cement pastes, primarily at the early stage. Compared to FA50, CFA50 exhibits 98.97 % and 113.41 % higher compressive strengths at 1 and 3 days, respectively. The carbonation treatment can significantly decrease the f-CaO content in class C FA, thereby enhancing volume stability.

(3) Compared with FA blended cement, the following factors can be attributed to the early improvement in strength with CFA: i) CFA can improve the amount and density of outer hydration products. Further, calcite can provide active nucleation sites for hydrates and participate in

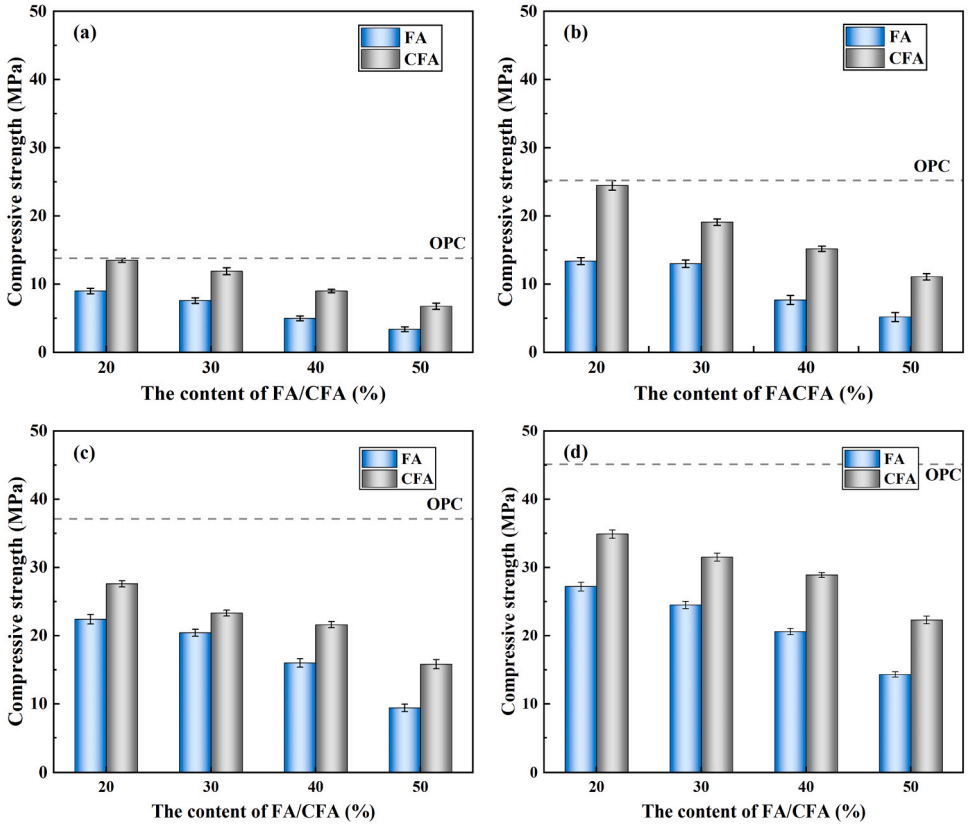

Fig. 20. Compressive strength development of FA/CFA pastes: (a) 1 day; (b) 3 days; (c) 7 days; (d) 28 days.

Table 7
Compressive strength of per kilogram cement.

Compressive strength per kg cement	1 day (MPa/kg)	3 days (MPa/kg)	7 days (MPa/kg)	28 days (MPa/kg)
OPC	33.75	67	92.75	103.75
FA20	28.13	41.88	70	85.00
CFA20	42.19	76.56	86.25	109.06
FA30	27.14	46.43	72.86	87.50
CFA30	42.50	68.21	83.21	112.50
FA40	20.83	32.08	66.67	85.83
CFA40	37.50	63.33	90.00	120.42
FA50	17.00	26.00	47.00	71.50
CFA50	33.82	55.50	79.00	111.50

the formation of Mc and Hc to improve the density of CFA paste. ii) It is possible to improve the strength of FA pastes by optimizing the pore structure and densifying the microstructure using CFA.

CO_2 carbonization of FA and its application as SCMs can enhance the reactivity of FA and decrease the quantity of cement required, which can be a sustainable and economical solution to reduce carbon emissions in the cement industry. Nevertheless, further research on the influence of carbonated FA on the mechanical, workability, and durability properties of concrete is required for the applications on large-scale concrete, an area to be further explored.

CRediT authorship contribution statement

Shao Yingxuan: Investigation, Data curation. **Fang Haibo:** Methodology, Conceptualization. **Xue Xingjie:** Writing – original draft, Investigation, Data curation. **Šavija Branko:** Formal analysis, Conceptualization. **Zhang Hongzhi:** Writing – review & editing, Investigation, Data curation. **Sun Ke:** Methodology, Investigation. **Ge Zhi:** Methodology, Investigation.

Declaration of Competing Interest

The authors declare that they have no known competing financial interests or personal relationships that could have influenced the work reported in this paper.

Acknowledgements

This work was supported by the Key Basic Research Project of China (No. 2022YFC3005604), "Unveiling and Commanding" Project of Jinan Science and Technology Bureau (No. 202323004), 111 Project (No. B21012), National Natural Science Foundation of China (No. 52378250), Taishan Scholars Foundation of Shandong Province (No. tsqn201909032), Natural Science Foundation of Shandong Province (No. ZR2024ME113).

Data Availability

Data will be made available on request.

References

[1] X. Liu, L. Yang, J. Du, H. Zhang, J. Hu, A. Chen, W. Lv, Carbon and air pollutant emissions forecast of China's cement industry from 2021 to 2035, Resour., Conserv. Recycl. 204 (2024) 107498.
[2] K. Wojtacha-Rychter, P. Kucharski, A. Smolinski, Conventional and alternative sources of thermal energy in the production of cement—an impact on CO2 emission, Energies 14 (6) (2021) 1539.
[3] S. Nie, J. Zhou, F. Yang, M. Lan, J. Li, Z. Zhang, Z. Chen, M. Xu, H. Li, J. G. Sanjayan, Analysis of theoretical carbon dioxide emissions from cement production: methodology and application, J. Clean. Prod. 334 (2022) 130270.
[4] A. Hasanbeigi, L. Price, E.J.R. Lin, S.E. Reviews, Emerging energy-efficiency and CO2 emission-reduction technologies for cement and concrete production, A Tech. Rev. 16 (8) (2012) 6220–6238.

[5] J. Du, Z. Liu, C. Christodoulatos, M. Conway, Y. Bao, W. Meng, Utilization of off-specification fly ash in preparing ultra-high-performance concrete (UHPC): Mixture design, characterization, and life-cycle assessment, Resour., Conserv. Recycl. 180 (2022) 106136.
[6] P. Payakaniti, N. Chuewangkam, R. Yensano, S. Pinitsoontorn, P. Chindaprasirt, Changes in compressive strength, microstructure and magnetic properties of a high-calcium fly ash geopolymer subjected to high temperatures, Constr. Build. Mater. 265 (2020) 120650.
[7] X.-Y. Wang, Embodied CO2-based optimal design of concrete with fly ash considering stress and carbonation, J. Sustain. Cem. -Based Mater. 12 (1) (2022) 71–82.
[8] D. Pushpalal, S. Danzandorj, N. Bayarjavkhlan, T. Nishiwaki, K. Yamamoto, Compressive strength development and durability properties of high-calcium fly ash incorporated concrete in extremely cold weather, Constr. Build. Mater. 316 (2022) 125801.
[9] M. Moradian, Q. Hu, M. Aboustait, B. Robertson, M.T. Ley, J.C. Hanan, X. Xiao, Direct in-situ observation of early age void evolution in sustainable cement paste containing fly ash or limestone, Compos. Part B: Eng. 175 (2019).
[10] P. Van den Heede, N.De Belie, Environmental impact and life cycle assessment (LCA) of traditional and 'green' concretes: literature review and theoretical calculations, Cem. Concr. Compos. 34 (4) (2012) 431–442.
[11] J. Zhang, S. Zhang, B. Liu, Degradation technologies and mechanisms of dioxins in municipal solid waste incineration fly ash: a review, J. Clean. Prod. 250 (2020) 119507.
[12] M. Sadique, H. Al-Nageim, Hydration kinetics of a low carbon cementitious material produced by physico-chemical activation of high calcium fly ash, J. Adv. Concr. Technol. 10 (8) (2012) 254–263.
[13] S. Aydın, Ç . Karatay, B. Baradan, The effect of grinding process on mechanical properties and alkali–silica reaction resistance of fly ash incorporated cement mortars, Powder Technol. 197 (1-2) (2010) 68–72.
[14] T. He, Y. Da, R. Xu, R. Yang, Effect of multiple chemical activators on mechanical property of high replacement high calcium fly ash blended system, Constr. Build. Mater. 198 (2019) 537–545.
[15] X. Hu, P. He, C. Shi, Carbonate binders: Historic developments and perspectives, Cem. Concr. Res. 175 (2024) 107352.
[16] M. Zajac, I. Maruyama, A. Iizuka, J. Skibsted, Enforced carbonation of cementitious materials, Cem. Concr. Res. 174 (2023) 107285.
[17] X. Fang, D. Xuan, P. Shen, C.S. Poon, Fast enhancement of recycled fine aggregates properties by wet carbonation, J. Clean. Prod. 313 (2021) 127867.
[18] W. Liu, L. Teng, S. Rohani, Z. Qin, B. Zhao, C.C. Xu, S. Ren, Q. Liu, B. Liang, CO2 mineral carbonation using industrial solid wastes: a review of recent developments, Chem. Eng. J. 416 (2021) 129093.
[19] C. Liang, B. Pan, Z. Ma, Z. He, Z. Duan, Utilization of CO2 curing to enhance the properties of recycled aggregate and prepared concrete: a review, Cem. Concr. Compos. 105 (2020) 103446.
[20] E.R. Bobicki, Q. Liu, Z. Xu, H. Zeng, Carbon capture and storage using alkaline industrial wastes, Prog. Energy Combust. Sci. 38 (2) (2012) 302–320.
[21] C. Siriruang, P. Toochinda, P. Julnipitawong, S. Tangtermsirikul, CO2 capture using fly ash from coal fired power plant and applications of CO2-captured fly ash as a mineral admixture for concrete, J. Environ. Manag. 170 (2016) 70–78.
[22] A. Ebrahimi, M. Saffari, D. Milani, A. Montoya, M. Valix, A. Abbas, Sustainable transformation of fly ash industrial waste into a construction cement blend via CO2 carbonation, J. Clean. Prod. 156 (2017) 660–669.
[23] T. Chen, M. Bai, X. Gao, Carbonation curing of cement mortars incorporating carbonated fly ash for performance improvement and CO2 sequestration, J. CO2 Util. 51 (2021) 101633.
[24] G. Deng, N. Zhang, W. Liao, H. Ma, Y. He, L. Lu, L. Chi, Pozzolanic reactivity of carbonated high-calcium fly ash: a mechanism study, Constr. Build. Mater. 446 (2024) 138015.
[25] R.R.T. Dananjayan, P. Kandasamy, R. Andimuthu, Direct mineral carbonation of coal fly ash for CO2 sequestration, J. Clean. Prod. 112 (2016) 4173–4182.
[26] W. Liu, S. Su, K. Xu, Q. Chen, J. Xu, Z. Sun, Y. Wang, S. Hu, X. Wang, Y. Xue, CO2 sequestration by direct gas–solid carbonation of fly ash with steam addition, J. Clean. Prod. 178 (2018) 98–107.
[27] K. Rausis, A. Ćwik, I. Casanova, K. Zarębska, Carbonation of high-Ca fly ashes under flue gas conditions: implications for their valorization in the construction industry, Crystals 11 (11) (2021) 1314.
[28] A. Dindi, D.V. Quang, L.F. Vega, E. Nashef, M.R. Abu-Zahra, Applications of fly ash for CO2 capture, utilization, and storage, J. CO2 Util. 29 (2019) 82–102.
[29] C. Wang, H. Jiang, E. Miao, Y. Wang, T. Zhang, Y. Xiao, Z. Liu, J. Ma, Z. Xiong, Y. Zhao, Accelerated CO2 mineralization technology using fly ash as raw material: recent research advances, Chem. Eng. J. (2024) 150676.
[30] Q. Yuan, G. Yang, Y. Zhang, T. Wang, J. Wang, C.E. Romero, Supercritical CO2 coupled with mechanical force to enhance carbonation of fly ash and heavy metal solidification, Fuel 315 (2022) 123154.
[31] L. Ji, H. Yu, X. Wang, M. Grigore, D. French, Y.M. Gözükara, J. Yu, M. Zeng, CO2 sequestration by direct mineralisation using fly ash from Chinese Shenfu coal, Fuel Process. Technol. 156 (2017) 429–437.
[32] N.L. Ukwattage, P. Ranjith, M. Yellishetty, H.H. Bui, T. Xu, A laboratory-scale study of the aqueous mineral carbonation of coal fly ash for CO2 sequestration, J. Clean. Prod. 103 (2015) 665–674.
[33] X. Shao, B. Qin, Q. Shi, Y. Yang, Z. Ma, Y. Li, Z. Jiang, W. Jiang, The impacts of CO2 mineralization reaction on the physicochemical characteristics of fly ash: a study under different reaction conditions of the water-to-solid ratio and the pressure of CO2, Energy 287 (2024) 129676.
[34] Q. Yuan, X. Guo, S. Ma, The influence mechanism of mechanical modification on fly ash carbonation to solidify heavy metals, J. Environ. Chem. Eng. 12 (6) (2024) 114714.
[35] Standard Specification for Coal Fly Ash and Raw or Calcined Natural Pozzolan for Use in Concrete, ASTM C. (1994) 618–622.
[36] A. Ćwik, I. Casanova, K. Rausis, N. Koukouzas, K. Zarębska, Carbonation of high-calcium fly ashes and its potential for carbon dioxide removal in coal fired power plants, J. Clean. Prod. 202 (2018) 1026–1034.
[37] C. Hu, Z. Li, Micromechanical investigation of Portland cement paste, Constr. Build. Mater. 71 (2014) 44–52.
[38] J.-X. Lu, P. Shen, Y. Zhang, H. Zheng, Y. Sun, C.S. Poon, Early-age and microstructural properties of glass powder blended cement paste: improvement by seawater, Cem. Concr. Compos. 122 (2021) 104165.
[39] M. Liang, S. He, Y. Gan, H. Zhang, Z. Chang, E. Schlangen, B. Šavija, Predicting micromechanical properties of cement paste from backscattered electron (BSE) images by computer vision, Mater. Des. 229 (2023) 111905.
[40] H. Zhang, Y. Xu, Y. Gan, Z. Chang, E. Schlangen, B. Šavija, Combined experimental and numerical study of uniaxial compression failure of hardened cement paste at micrometre length scale, Cem. Concr. Res. 126 (2019) 105925.
[41] L. Ji, H. Yu, B. Yu, R. Zhang, D. French, M. Grigore, X. Wang, Z. Chen, S. Zhao, Insights into carbonation kinetics of fly ash from victorian lignite for CO2 sequestration, Energy Fuels 32 (4) (2018) 4569–4578.
[42] X. Shao, B. Qin, Q. Shi, Y. Yang, Z. Ma, Y. Li, Z. Jiang, W. Jiang, The impacts of CO2 mineralization reaction on the physicochemical characteristics of fly ash: a study under different reaction conditions of the water-to-solid ratio and the pressure of CO2, Energy 287 (2024).
[43] J. Jaschik, M. Jaschik, K. Warmuziński, The utilisation of fly ash in CO2 mineral carbonation, Chem. Process Eng. 37 (1) (2016) 29–39.
[44] P. He, S. Drissi, X. Hu, J. Liu, C. Shi, Investigation on the influential mechanism of FA and GGBS on the properties of CO2-cured cement paste, Cem. Concr. Compos. (2023) 142.
[45] D. Wang, Y. Fang, Y. Zhang, J. Chang, Changes in mineral composition, growth of calcite crystal, and promotion of physico-chemical properties induced by carbonation of β-C2S, J. CO2 Util. 34 (2019) 149–162.
[46] C.S. Poon, P. Shen, Y. Jiang, Z. Ma, D. Xuan, Total recycling of concrete waste using accelerated carbonation: a review, Cem. Concr. Res. 173 (2023) 107284.
[47] Y. Zhang, L. Yu, K. Cui, H. Wang, T. Fu, Carbon capture and storage technology by steel-making slags: recent progress and future challenges, Chem. Eng. J. 455 (2023) 140552.
[48] K.E. Gomari, S.R. Gomari, D. Hughes, T. Ahmed, Exploring the potential of steel slag waste for carbon sequestration through mineral carbonation: a comparative study of blast-furnace slag and ladle slag, J. Environ. Manag. 351 (2024) 119835.
[49] T. Hemalatha, A.J.Jocp Ramaswamy, A review on fly ash characteristics–Towards promoting high volume utilization in developing sustainable concrete, 147 (2017) 546-559.
[50] K. De Weerdt, M.B. Haha, G. Le Saout, K.O. Kjellsen, H. Justnes, B.J.C. Lothenbach, C. Research, Hydration mechanisms of ternary Portland cements containing limestone powder and fly ash 41 (3) (2011) 279–291.
[51] K. Scrivener, R. Snellings, B. Lothenbach, A Practical Guide To Microstructural Analysis Of Cementitious Materials, Crc Press, Boca Raton, FL, USA, 2016.
[52] Y. Li, S. Eyley, W. Thielemans, Q. Yuan, J. Li, Valorization of deep soil mixing residue in cement-based materials, Resour., Conserv. Recycl. 187 (2022).
[53] S.-Y. Pan, E.-E. Chang, H. Kim, Y.-H. Chen, P.-C. Chiang, Validating carbonation parameters of alkaline solid wastes via integrated thermal analyses: Principles and applications, J. Hazard. Mater. 307 (2016) 253–262.
[54] X. Zheng, J. Liu, Y. Wei, K. Li, H. Yu, X. Wang, L. Ji, S. Yan, Glycine-mediated leaching-mineralization cycle for CO2 sequestration and CaCO3 production from coal fly ash: Dual functions of glycine as a proton donor and receptor, Chem. Eng. J. 440 (2022) 135900.
[55] L.L. He, D.X. Yu, W.Z. Lv, J.Q. Wu, M.H. Xu, CO2 sequestration by indirect carbonation of high-calcium coal fly ash, Adv. Mater. Res. 726 (2013) 2870–2874.
[56] E. Chang, S.-Y. Pan, L. Yang, Y.-H. Chen, H. Kim, P.-C. Chiang, Accelerated carbonation using municipal solid waste incinerator bottom ash and cold-rolling wastewater: Performance evaluation and reaction kinetics, Waste Manag. 43 (2015) 283–292.
[57] S.-J. Han, H.J. Im, J.-H. Wee, Leaching and indirect mineral carbonation performance of coal fly ash-water solution system, Appl. Energy 142 (2015) 274–282.
[58] L.J. Gardner, S.A. Bernal, S.A. Walling, C.L. Corkhill, J.L. Provis, N.C. Hyatt, Characterisation of magnesium potassium phosphate cements blended with fly ash and ground granulated blast furnace slag, Cem. Concr. Res. 74 (2015) 78–87.
[59] Q. Fu, Z. Zhang, X. Zhao, W. Xu, D. Niu, Effect of nano calcium carbonate on hydration characteristics and microstructure of cement-based materials: A review, J. Build. Eng. 50 (2022) 104220.
[60] T. Sato, J.J. Beaudoin, Effect of nano-CaCO3 on hydration of cement containing supplementary cementitious materials, Adv. Cem. Res. 23 (1) (2011) 33–43.
[61] L. Peng, Y. Jiang, J. Ban, Y. Shen, Z. Ma, Y. Zhao, P. Shen, C.-S.J.C. Poon, C. Composites, Mechanism underlying early hydration kinetics of carbonated recycled concrete fines-ordinary portland cement (CRCF-OPC) paste, 144 (2023) 105275.
[62] K. Yan, F. Gao, H. Sun, D. Ge, S. Yang, Effects of municipal solid waste incineration fly ash on the characterization of cement-stabilized macadam, Constr. Build. Mater. 207 (2019) 181–189.
[63] K. Lin, K. Wang, B. Tzeng, C. Lin, The hydration characteristics and utilization of slag obtained by the vitrification of MSWI fly ash, Waste Manag. 24 (2) (2004) 199–205.

[64] Z. Yuan, Z. Pang, C. Lu, Y. Yao, Feasibility study of engineered geopolymer composites based high-calcium fly ash and micromechanics analysis, Case Stud. Constr. Mater. 20 (2024) e02701.
[65] J. Makar, G. Chan, K. Esseghaier, A peak in the hydration reaction at the end of the cement induction period, J. Mater. Sci. 42 (2007) 1388–1392.
[66] B. Lu, C. Shi, J. Zhang, J. Wang, Effects of carbonated hardened cement paste powder on hydration and microstructure of Portland cement, Constr. Build. Mater. 186 (2018) 699–708.
[67] D.P. Bentz, C.F. Ferraris, S.Z. Jones, D. Lootens, F. Zunino, Limestone and silica powder replacements for cement: Early-age performance, Cem. Concr. Compos. 78 (2017) 43–56.
[68] Y. Su, H. Zhao, X. He, Z. Zheng, Q. Ma, J. Ding, M. Bao, The effect of wet-grinding phosphorus slag on the hydration kinetics of Portland cement, Constr. Build. Mater. 364 (2023) 129942.
[69] G. Zhang, H. Xia, H. Wang, L. Song, Y. Niu, D. Cao, H. Chen, Early hydration characteristics and kinetics model of cement pastes containing internal curing materials with different absorption behaviors, Constr. Build. Mater. 383 (2023) 131412.
[70] S. Meng, Z. Shi, X. Ouyang, Comparison of the effects of carbon-based and inorganic nanomaterials on early cement hydration, Constr. Build. Mater. 421 (2024) 135705.
[71] S. Liu, L. Wang, Y. Gao, B. Yu, W. Tang, Influence of fineness on hydration kinetics of supersulfated cement, Thermochim. Acta 605 (2015) 37–42.
[72] M. Zajac, A. Rossberg, G. Le Saout, B. Lothenbach, Influence of limestone and anhydrite on the hydration of Portland cements, Cem. Concr. Compos. 46 (2014) 99–108.
[73] Y. Wu, H. Mehdizadeh, K.H. Mo, T.-C. Ling, High-temperature CO2 for accelerating the carbonation of recycled concrete fines, J. Build. Eng. 52 (2022) 104526.
[74] K. De Weerdt, M.B. Haha, G. Le Saout, K.O. Kjellsen, H. Justnes, B. Lothenbach, Hydration mechanisms of ternary Portland cements containing limestone powder and fly ash, Cem. Concr. Res. 41 (3) (2011) 279–291.
[75] T. Matschei, B. Lothenbach, P.F. Glasser, The role of calcium carbonate in cement hydration, Cem. Concr. Res. (2007).
[76] B. Lothenbach, G.L. Saout, E. Gallucci, K. Scrivener, Influence of limestone on the hydration of Portland cements, Cem. Concr. Res. 38 (6) (2008) 339–356.
[77] Y. Li, T. Mi, W. Liu, Z. Dong, B. Dong, L. Tang, F. Xing, Chemical and mineralogical characteristics of carbonated and uncarbonated cement pastes subjected to high temperatures, Compos. Part B: Eng. 216 (2021).
[78] C. Li, S. Krishnya, M. Ogino, E. Owaki, Y.J.C. Elakneswaran, B. Materials, Investigating the hydration characteristics of a new composite cementitious binder containing of slag and calcite, 361 (2022) 129629.
[79] K. Cui, D. Lau, Y. Zhang, J.J.C. Chang, B. Materials, Mechanical properties and mechanism of nano-CaCO3 enhanced sulphoaluminate cement-based reactive powder concrete, 309 (2021) 125099.
[80] F. Georget, B. Lothenbach, W. Wilson, F. Zunino, K.L. Scrivener, Stability of hemicarbonate under cement paste-like conditions, Cem. Concr. Res. 153 (2022) 106692.
[81] E. Kuzielová, M. Slaný, M. Žemlička, J. Másilko, M.T. Palou, Phase composition of silica fume—portland cement systems formed under hydrothermal curing evaluated by ftir, xrd, and tga, Materials 14 (11) (2021) 2786.
[82] Z. Fengchen, M. Baoguo, W. Shengxing, Z. Jikai, Effect of Fly Ash on TSA Resistance of Cement-based Material, J. WUHAN Univ. Technol.-Mater. Sci. Ed. 26 (3) (2011) 561–566.
[83] C. Luan, Z. Wu, Z. Han, X. Gao, Z. Zhou, P. Du, F. Wu, S. Du, Y. Huang, The effects of calcium content of fly ash on hydration and microstructure of ultra-high performance concrete (UHPC), J. Clean. Prod. 415 (2023) 137735.
[84] S. Li, Y. Zhang, S. Lin, J. Yan, S.J.C. Du, B. Materials, Effects of nano-SiO2 coated multi-walled carbon nanotubes on mechanical properties of cement-based composites, 281 (2021) 122577.
[85] H. Yang, Y. Che, F. Leng, High volume fly ash mortar containing nano-calcium carbonate as a sustainable cementitious material: microstructure and strength development, Sci. Rep. 8 (1) (2018) 16439.
[86] E. L'Hôpital, B. Lothenbach, D.A. Kulik, K. Scrivener, Influence of calcium to silica ratio on aluminium uptake in calcium silicate hydrate, Cem. Concr. Res. 85 (2016) 111–121.
[87] J. Li, W. Zhang, P.J. Monteiro, Structure and intrinsic mechanical properties of nanocrystalline calcium silicate hydrate, ACS Sustain. Chem. Eng. 8 (33) (2020) 12453–12461.
[88] C. Luan, Y. Zhou, Y. Liu, Z. Ren, J. Wang, L. Yuan, S. Du, Z. Zhou, Y. Huang, Effects of nano-SiO2, nano-CaCO3 and nano-TiO2 on properties and microstructure of the high content calcium silicate phase cement (HCSC), Constr. Build. Mater. 314 (2022) 125377.
[89] H. Jun-Yuan, B.E. Scheetz, D.M. Roy, Hydration of fly ash-Portland cements, Cem. Concr. Res. 14 (4) (1984) 505–512.
[90] E.E. Berry, R.T. Hemmings, M.-H. Zhang, B.J. Cornelius, D.M. Golden, Hydration in high-volume fly ash concrete binders, Mater. J. 91 (4) (1994) 382–389.
[91] F. Chen, Study on freeze-thaw damage performance and characterisation of superabsorbent polymer cement mortars, Harbin Institute of Technology, 2021.
[92] F. Moghaddam, V. Sirivivatnanon, K. Vessalas, The effect of fly ash fineness on heat of hydration, microstructure, flow and compressive strength of blended cement pastes, Case Stud. Constr. Mater. 10 (2019) e00218.
[93] B. Lothenbach, T. Matschei, G.R. M?Schner, F.P. Glasser, Thermodynamic modelling of the effect of temperature on the hydration and porosity of Portland cement, Cem. Concr. Res. 38 (1) (2008) 1–18.